Journal of Molecular Liquids 218 (2016) 434–456

Contents lists available at ScienceDirect

Journal of Molecular Liquids

journal homepage: www.elsevier.com/locate/molliq

Molecular docking, DNA binding, thermal studies and antimicrobial activities of Schiff base complexes

A.Z. El-Sonbati [a], M.A. Diab [a,*], A.A. El-Bindary [a], M.I. Abou-Dobara [b], H.A. Seyam [a]

[a] Chemistry Department, Faculty of Science, Damietta University, Damietta, Egypt
[b] Botany Department, Faculty of Science, Damietta University, Damietta, Egypt

ARTICLE INFO

Article history:
Received 24 January 2016
Received in revised form 7 February 2016
Accepted 22 February 2016
Available online xxxx

Keywords:
Schiff base
Molecular docking
DNA binding
Molecular structure
Thermodynamic parameters
Antioxidant and antitumor activity

ABSTRACT

Metal(II) complexes of 3-[(2-hydroxy-3-methoxybenzylidene)hydrazo]-1,3-dihydroindol-2-one (HL) were prepared, their compositions and physicochemical properties were characterized on the basis of elemental analysis, molar conductivity, ^{1}H NMR, UV–Vis, IR, mass spectroscopy, X-ray, magnetic measurements and thermogravimetric analysis (TGA). All results confirm that the novel complexes have 1:1 metal-to-ligand stoichiometric formulae [M(HL)(OAc)$_2$(OH$_2$)$_2$] (M═Cu(II)(**1**), Co(II)(**2**), Ni(II)(**3**) and Cd(II)(**4**)), octahedral configuration and the ligand behaves as a neutral bidentate forming six-membered chelating ring towards the metal ions, bonding through azomethine nitrogen and ketonic oxygen atoms. The molecular structures of the ligand and its metal complexes were also studied using quantum chemical calculations and shows that the keto form with hydrogen bond is more stable than other forms. The coordination geometry around all complexes (**1**–**4**) exhibits an octahedral geometry. The XRD studies show that both the ligand and Cu(II) complex show polycrystalline with Triclinic crystal system. The activation thermodynamic parameters, such as activation energy (E$_a$), enthalpy (ΔH), entropy (ΔS), and Gibbs free energy change of the decomposition (ΔG) are calculated using Coats–Redfern and Horowitz–Metzger methods. The ligand and its metal complexes (**1**–**4**) showed antimicrobial activity against bacterial species, Gram positive (*Staphylococcus aureus*), Gram negative (*Escherichia coli*) bacteria and yeast (*Candida albicans*), the ligand exhibited higher activity than the complexes. All investigated compounds were screened in vitro for their antioxidant, cytotoxic and antitumor activity. Molecular docking was used to predict the binding between HL ligand and the receptors of crystal structure of *E. coli* (3T88), crystal structure of *S. aureus* (3q8u) and crystal structure of *C. albicans* (1Q40).

1. Introduction

Schiff bases form an important class of organic compounds with a wide variety of biological properties [1–5]. Schiff bases, derived from various heterocycles, were reported to possess cytotoxic [6], anticancer, and antifungal activities [7]. Isatin (1H-indole-2,3-dione) was first discovered by Erdmann and Laurent in 1840 as a product of indigo oxidation [8,9]. Isatin have also been recognized in natural products, such as in humans as it is a metabolic derivative of adrenaline, marine molluscs, fungal metabolites [10–12]. Isatin and its analogs are versatile substrates, which can be used for the synthesis of numerous heterocyclic compounds. The synthetic ingenuity of isatin has led to the wide use of this compound in organic synthesis which reported to possess a variety of pharmacological properties such as antiviral activities, antibacterial, anticancer activities, anticonvulsant activity, cytotoxicity antioxidant activity [13–20]. Isatin derivatives have been used as important intermediates in organic synthesis [21]. Isatin is an important component of many alkaloids [22], drugs [23], dyes [24], pesticides, and analytical reagents.

Although metal complexes of monohydrazones derived from isatin have been extensively investigated, those formed from bishydrazones have received comparatively less attention so far [25–27].

Thereby, in the present study, we report the synthesis of 3-[(2-hydroxy-3-methoxy-benzylidene)-hydrazono]-1,3-dihydro-indol-2-one and its metal [Cu(II), Co(II), Ni(II) and Cd(II)] complexes. Also we report the structure characterization by different spectroscopic techniques. Antimicrobial activities, antioxidant and antitumor activity were studied. The calf thymus DNA binding activity of the ligand and its metal complexes were studied by absorption spectra. The thermogravimetric analysis (TGA) studies were done for the investigated compounds. In addition to the activation thermodynamic parameters are calculated using Coats–Redfern and Horowitz–Metzger methods. Study the molecular structures of the investigated compound. Study the docking of Schiff base ligand. In our laboratories,

* Corresponding author.
E-mail address: m.adiab@yahoo.com (M.A. Diab).

http://dx.doi.org/10.1016/j.molliq.2016.02.072
0167-7322/

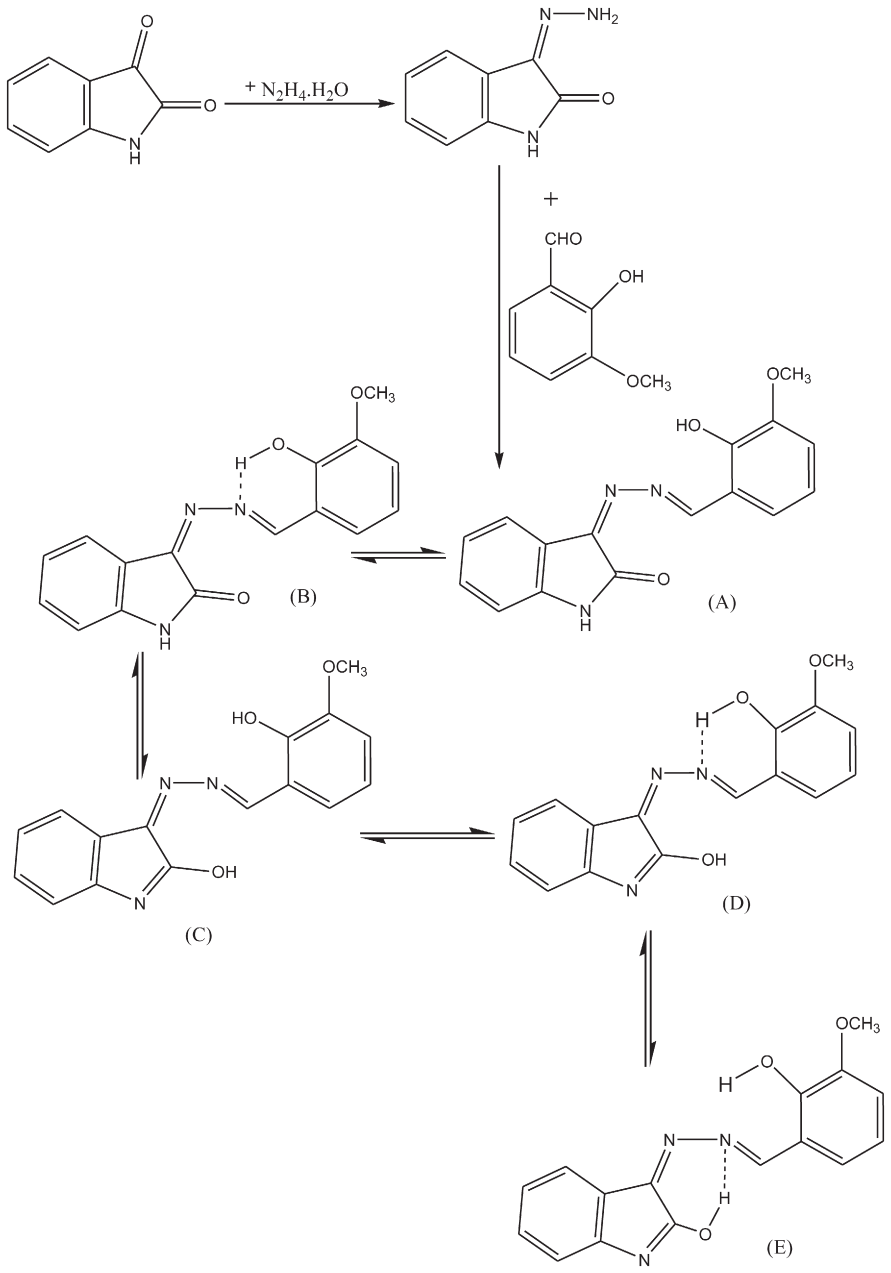

Scheme 1. Synthetic route of Schiff base ligand (A) keto form, (B) keto form with hydrogen bond, (C) enol form, (D) enol form with hydrogen bond and (E) enol form with hydrogen bond.

the chemical equilibria and although the coordination complexes of HL (Scheme 1) has been extensively investigated [28–31], no attention has been paid to the HL or to the metal complexes of the HL.

2. Experimental

2.1. Materials

All reactants (Isatin, Metals acetate, Hydrazine and aldehyde) were purchased from Aldrich, and were used without any further purification. CT-DNA was purchased from SRL (India). Double distilled water was used to prepare all buffer solutions. Cell line Hepatocellular carcinoma (HepG-2) and mammary gland breast cancer (MCF-7). The cell line was obtained from ATCC via Holding company for biological products and vaccines (VACSERA), Cairo, Egypt. 5-Fluorouracil was used as a standard anticancer drug for comparison. The reagents RPMI-1640 medium, MTT, DMSO and 5-fluorouracil (sigma co., St. Louis, USA), Fetal Bovine serum (GIBCO, UK).

2.2. Preparation of Schiff base ligand (HL)

Schiff base was prepared from ethanolic solutions of isatin and hydrazine hydrate in equimolar amount and were refluxed together for 30 min to afford hydrazone. Then condensation of hydrazine with 2-hydroxy-3-methoxy-benzaldehyde in equimolar amount in ethanol under reflux for 3 h, the excess solvent was removed by evaporation and the concentrated solution was cooled and filtration the powder of Schiff base was collected, then washed with ethanol. Recrystallization from ethanol afforded pure crystals. 3-[(2-hydroxy-3-methoxy-benzylidene)-hydrazono]-1,3-dihydro-indol-2-one. Yield: 80%. The

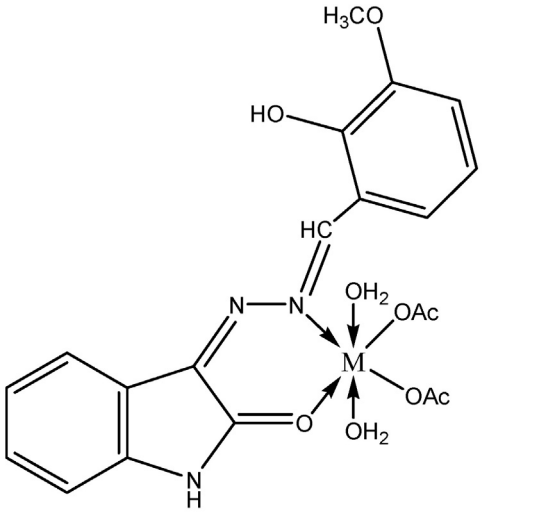

M = Cu(II) (1), Co(II) (2), Ni(II) (3), Cd(II) (4)

Fig. 1. The structure of the metal complexes (**1**–**4**).

purity of ligand was checked by TLC. Our synthetic route of Schiff base ligand is shown in Scheme 1.

2.3. Preparation of the complexes

The solid complexes (**1**–**4**) of the different metal ions under study were prepared and purified by recrystallization when possible (Fig. 1). The following synthetic has been employed.

Ethanolic solution of copper, cobalt, nickel or cadmium acetate (0.01) was added slowly to the stirred ligand mixture and the reaction mixture was further refluxed. The colored precipitates were filtered through sintered glass crucible and washed several times with hot ethanol, ether and finally dried in vacuum desiccator for 1 week.

2.4. DNA binding experiments

The binding properties of the ligand and complexes (**1**–**4**) to CT-DNA have been studied using electronic absorption spectroscopy. The stock solution of CT-DNA was prepared in 5 mM Tris–HCl/50 mM NaCl buffer (pH = 7.2), which a ratio of UV absorbances at 260 and 280 nm (A_{260}/A_{280}) of ca. 1.8–1.9, indicating that the DNA was sufficiently free of protein [32], and the concentration was determined by UV absorbance at 260 nm ($\varepsilon = 6600\ M^{-1}\ cm^{-1}$) [33]. Electronic absorption spectra (300–700 nm) were carried out using 1 cm quartz cuvettes at 25 °C by fixing the concentration of ligand or complex (1.00×10^{-3} mol L^{-1}), while gradually increasing the concentration of CT-DNA (0.00 to 1.30×10^{-4} mol·L^{-1}). An equal amount of CT-DNA was added to both the compound solutions and the references buffer solution to eliminate the absorbance of CT-DNA itself. The intrinsic binding constant K_b of the compound with CT-DNA was determined using the following equation [34]:

$$\frac{[DNA]}{(\varepsilon_a-\varepsilon_f)} = \frac{[DNA]}{(\varepsilon_b-\varepsilon_f)} + \frac{1}{K_b(\varepsilon_a-\varepsilon_f)} \quad (1)$$

where [DNA] is the concentration of CT-DNA in base pairs, ϵ_a is the extinction coefficient observed for the A_{obs}/[compound] at the given DNA concentration, ϵ_f is the extinction coefficient of the free compound in solution and ϵ_b is the extinction coefficient of the compound when fully bond to DNA. In plots of [DNA]/(ϵ_a–ϵ_f) versus [DNA], K_b is given by the ratio of the slope to the intercept.

2.5. Antimicrobial activity

Chemical compounds were individually tested against a Gram positive (*Staphylococcus aureus*), Gram negative (*Escherichia coli*) bacteria and yeast (*Candida albicans*). Each of the compounds was dissolved in DMSO and solution of the concentration 1 mg/mL were prepared separately and paper disks of Whatman filter paper were prepared with standard size (5 cm) were cut and sterilized in an autoclave. The paper disks were soaked in the desired concentration of the complex solution and were placed aseptically in the petri dishes containing nutrient agar media (agar 20 g, beef extract 3 g and peptone 5 g) seeded with *S. aureus*, *E. coli* and *C. albicans*. The petri dishes were incubated at 36 °C and the inhibition zones were recorded after 24 h of incubation. Each treatment was replicated three times. The antibacterial activity of a common standard antibiotic ampicillin and antifungal Clotrimazole was also recorded using the same procedure as above at the same concentration and solvents. The % activity index for the complex was calculated by the formula as under [35]:

$$\%\ \text{activity index} = \frac{\text{Zone of inhibition by test compound(diameter)}}{\text{Zone of inhibition by standard(diameter) x 100}}. \quad (2)$$

2.6. Antioxidant assay

Antioxidant activity determined by screening assay ABTS method. For each of the investigated compounds (2 mL) of ABTS solution (60 μM) was added to 3 mL MnO_2 solution (25 mg/mL), all prepared in (5 mL) aqueous phosphate buffer solution (pH 7, 0.1 M).The mixture was shaken, centrifuged, filtered and the absorbance of the resulting green blue solution (ABTS radical solution) at 734 nm was adjusted to approx. ca. 0.5. Then, 50 μl of (2 mM) solution of the tested compound in spectroscopic grade MeOH/phosphate buffer (1:1) was added. The absorbance was measured and the reduction in color intensity was expressed as inhibition percentage. L-ascorbic acid was used as standard antioxidant (Positive control). Blank sample was run without ABTS and using MeOH/phosphate buffer (1:1) instead of tested compounds. Negative control was run with ABTS and MeOH/phosphate buffer (1:1) only [36–38].

Table 1
Energy values obtained in docking calculations of ligand (HL) with receptors of crystal structure of *E. coli* (3T88), crystal structure of *S. aureus* (3q8u) and crystal structure of *C. albicans* (1Q40).

Receptors	Est. inhibition constant (Ki) (μM)	vdW + bond + desolve energy (kcal/mol)	Electrostatic energy (kcal/mol)	Total intercooled energy (kcal/mol)	Interact surface
3T88	25.34	−7.03	−0.06	−7.09	746.35
3q8u	88.45	−6.50	−0.15	−6.65	824.09
1Q40	128.65	−6.24	−0.08	−6.32	624.06

2.7. Cytotoxicity assay

The cell lines mentioned above were used to determine the inhibitory effects of compounds on cell growth using the MTT assay [39, 40]. This colorimetric assay is based on the conversion of the yellow tetrazolium bromide (MTT) to a purple formazan derivative by mitochondrial succinate dehydrogenase in viable cells. Cell lines were cultured in RPMI-1640 medium with 10% fetal bovine serum. Antibiotics added were 100 units/mL penicillin and 100 μg/mL streptomycin at 37 °C in a 5% CO_2 incubator. The cell lines were seeded in a 96-well plate at a density of 1.0×10^4 cells/well at 37 °C for 48 h under 5% CO_2, followed by 24 h incubation with the indicated drug doses [41]. In the end of drug treatment, 20 μl of MTT solution at 5 mg/mL was added and incubated for 4 h. Dimethylsulfoxide in

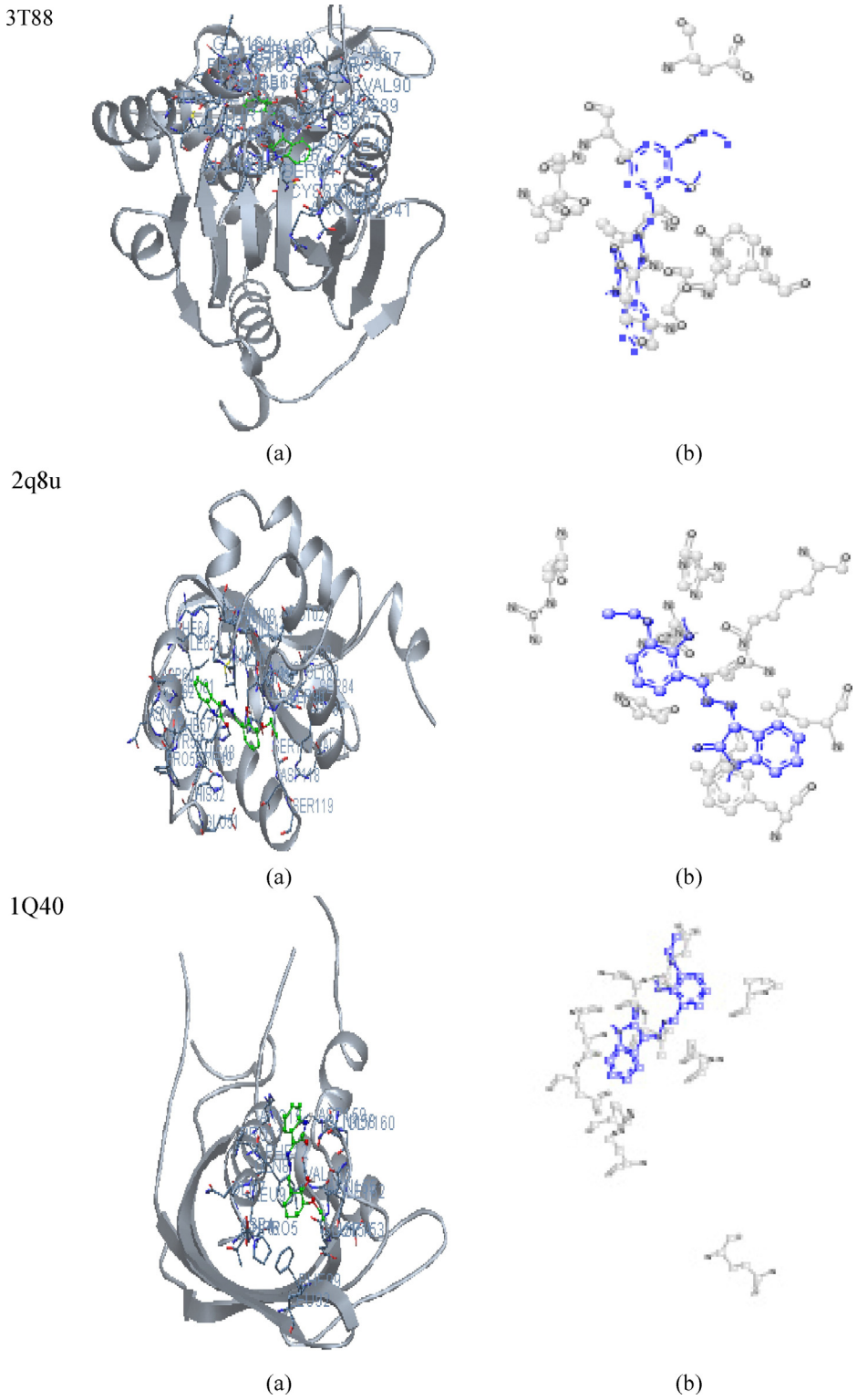

Fig. 2. The ligand HL (green in (a) and blue in (b)) in interaction with receptors of crystal structure of *E. coli* (3T88), crystal structure of *S. aureus* (3q8u) and crystal structure of *C. albicans* (1Q40). (For interpretation of the references to color in this figure legend, the reader is referred to the web version of this article).

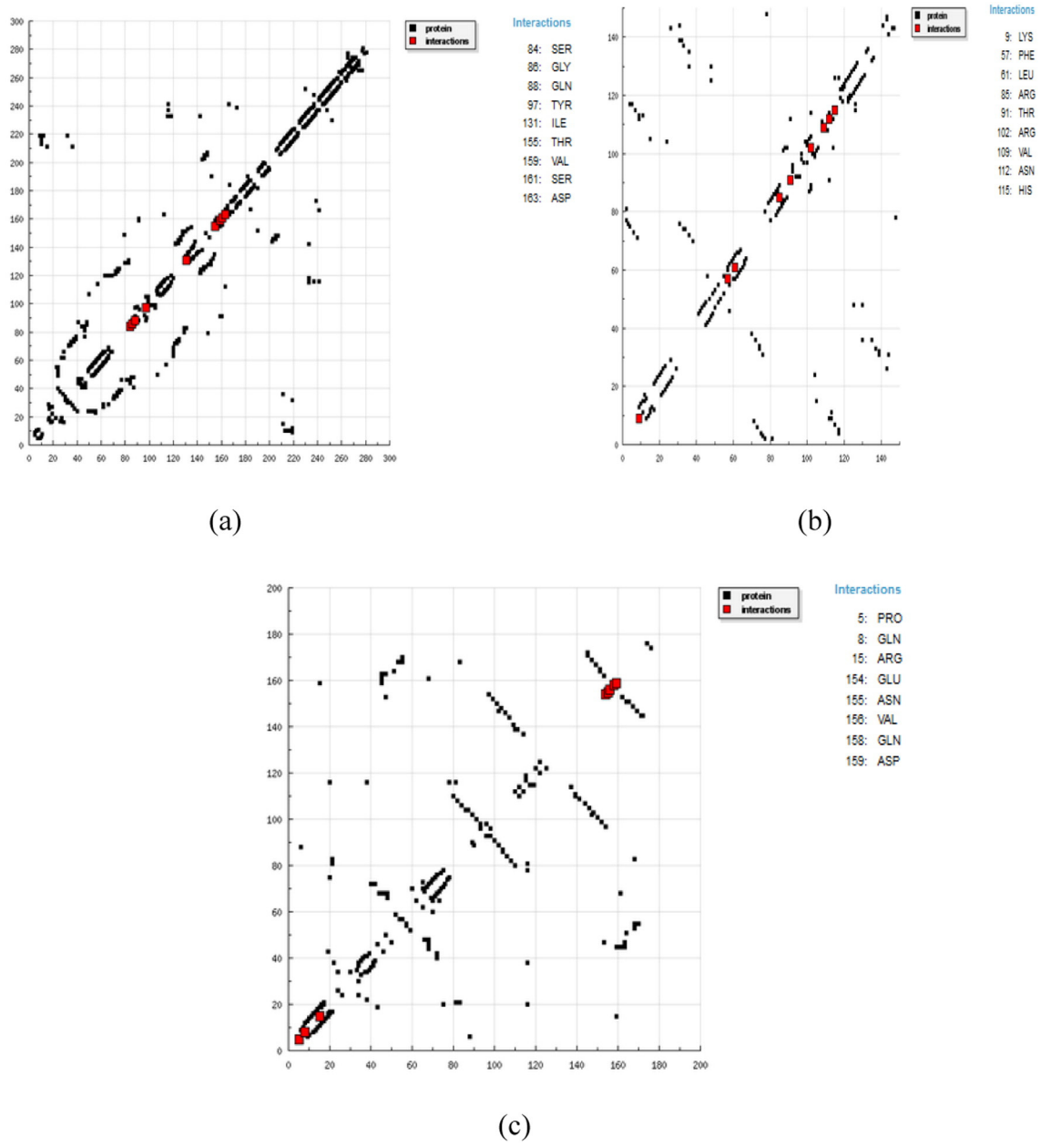

Fig. 3. HB plot of interaction between ligand HL and receptor (a) crystal structure of *E. coli* (3T88), (b) crystal structure of *S. aureus* (3q8u) and (c) crystal structure of *C. albicans* (1Q40).

volume of 100 μl is added into each well to dissolve the purple formazan formed. The colorimetric assay is measured and recorded at absorbance of 570 nm using a plate reader (EXL 800). The relative cell viability in percentage was calculated as (A570 of treated samples/A570 of untreated sample) × 100.

2.8. Measurements

Elemental microanalyses of the separated ligand and solid chelates for C, H, and N were performed on Perkin-Elmer (2400) CHNS analyzer. The analyses were repeated twice to check the accuracy of the analyzed data. The metal content in the complexes was estimated by standard methods [42]. Spectroscopic data were obtained using the following instruments: Ultraviolet–Visible (UV–Vis) spectra of the compounds were recorded using a Perkin-Elmer AA 800 spectrophotometer model AAS. Infrared spectra were recorded as KBr disks using a Pye Unicam SP 2000 spectrophotometer. The ^{1}H NMR spectrum was obtained with a Bruker WP 300 MHz using DMSO-d_6 as a solvent containing TMS as the internal standard. Mass spectra were recorded by the EI technique at 70 eV using MS-5988 GS–MS Hewlett-Packard. The magnetic moment of the prepared solid complexes was determined at room temperature using the Gouy's method. Mercury(II) (tetrathiocyanato)cobalt(II), [Hg{Co(SCN)$_4$}], was used for the calibration of the Gouy tubes. Diamagnetic corrections were calculated from the values given by Selwood [43] and Pascal's constants. Magnetic moments were calculated using the equation, $\mu_{eff.} = 2.84\,[T\chi_M^{coor.}]^{1/2}$. X-ray diffraction analysis of the ligand and its Copper complex powder forms was recorded on X-ray diffractometer in the range of diffraction angle $2\theta^\circ = 5–80^\circ$. This analysis was carried out using Cu Kα radiation ($\lambda = 1.540598$ Å). The applied voltage and the tube current are 40 kV and 30 mA, respectively. The diffraction peaks in powder spectra are indexed and the lattice parameters are determined with the aid of CRYSFIRE

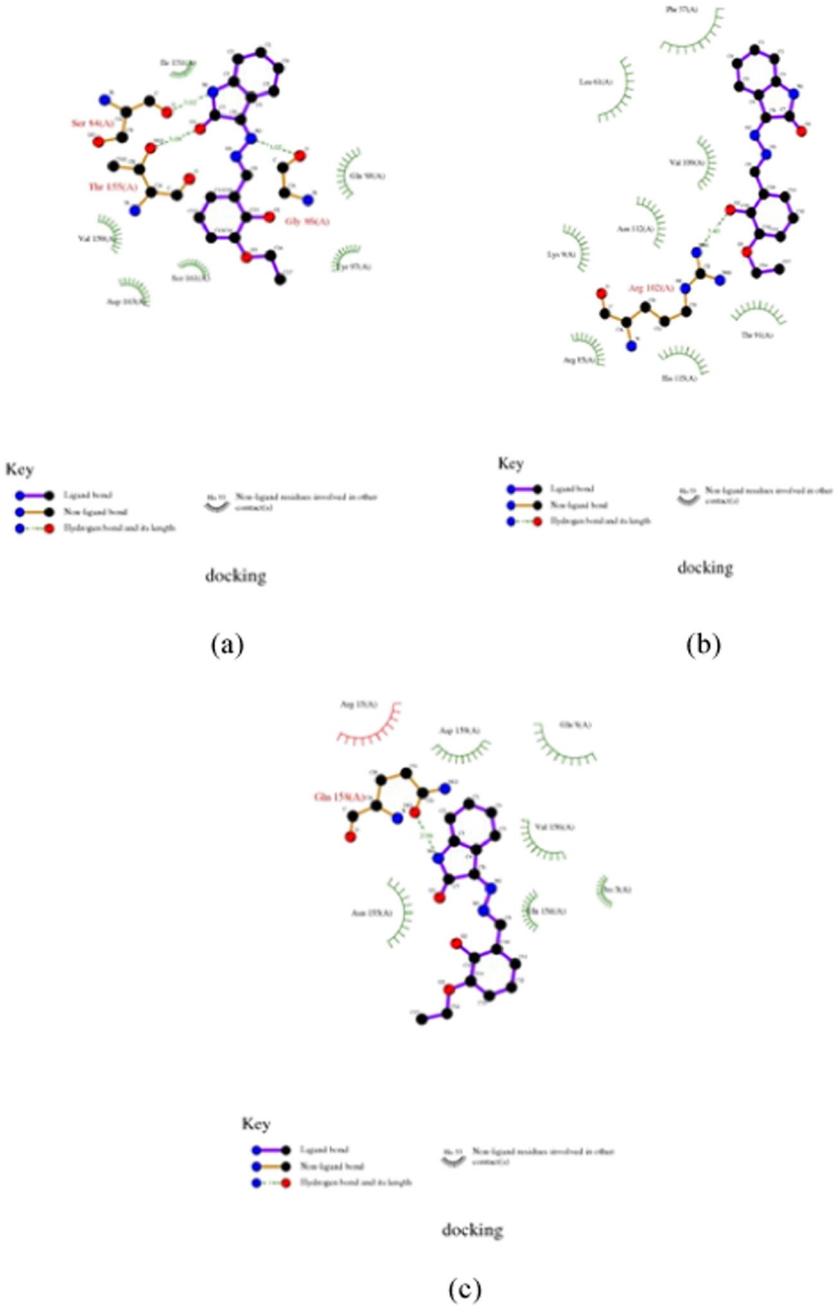

Fig. 4. 2D plot of interaction between ligand HL and receptor (a) crystal structure of *E. coli* (3T88), (b) crystal structure of *S. aureus* (3q8u) and (c) crystal structure of *C. albicans* (1Q40).

computer program [44]. The value of interplanar spacing, d, and Miller indices, *hkl*, for each diffraction peak are determined by using CHEKCELL program [45]. Thermal studies were computed on Simultaneous Thermal Analyzer (STA) 6000 system using thermogravimetric analysis (TGA) method. Thermal properties of the samples were analyzed in the temperature range up to 800 °C at the heating rate of 10 °C/min under dynamic nitrogen atmosphere. The molecular structures of the ligands were optimized by HF method with 3–21G basis set. The molecules were built with the Perkin Elmer ChemBioDraw and optimized using the Perkin Elmer ChemBio3D software [46,47].

Table 2
Elemental analyses data of metal complexes.

Compounds	Yield (%)	Exp. (Calcd.) (%)				μ_{eff} (B.M.)
		C	H	N	M	
$[Cu(HL)(OAc)_2(OH_2)_2]$ (**1**)	52.67	46.64 (46.83)	4.38 (4.49)	7.88 (8.19)	12.26 (12.40)	1.83
$[Co(HL)(OAc)_2(OH_2)_2]$ (**2**)	66.17	47.18 (47.25)	4.37 (4.53)	7.89 (8.27)	11.46 (11.60)	4.46
$[Ni(HL)(OAc)_2(OH_2)_2]$ (**3**)	65.50	47.15 (47.27)	4.33 (4.53)	7.87 (8.27)	11.37 (11.56)	3.35
$[Cd(HL)(OAc)_2(OH_2)_2]$ (**4**)	85.50	42.64 (42.75)	3.98 (4.10)	7.19 (7.48)	19.88 (20.02)	Dia.

Table 3
IR spectral bands of the ligand and its metal complexes[a].

(HL)	(**1**)	(**2**)	(**3**)	(**4**)	Assignments
3436	3444	3440	3441	3443	ν(OH)
3180	3185	3183	3186	3182	ν(NH)
1714	1645	1660	1660	1660	ν(C═O)
1617	1604	1589	1605	1607	ν(C═N)
1251	1248	1246	1245	1249	ν(C–O)
–	464	460	455	495	ν(M–O)
–	426	430	440	420	ν(M–N)

[a] Numbers given in Table 2.

In the study simulates the actual docking process in which the ligand–protein pair-wise interaction energies are calculated using Docking Server [48]. The MMFF94 Force field was for used energy minimization of ligand molecule using Docking Server. Gasteiger partial charges were added to the ligand atoms. Non-polar hydrogen atoms were merged, and rotatable bonds were defined. Docking calculations were carried out on crystal structure of *E. coli* (3T88), crystal structure of *S. aureus* (3q8u) and crystal structure of *C. albicans* (1Q40) model Essential hydrogen atoms, Kollman united atom type charges, and solvation parameters were added with the aid of AutoDock tools [49]. Auto Dock parameter set- and distance-dependent dielectric functions were used in the calculation of the van der Waals and the electrostatic terms, respectively.

3. Results and discussion

3.1. Characterization of ligand

The structure elucidation of the prepared Schiff base (HL) is carried out by using different techniques namely elemental analyses, UV–vis, IR, ^{1}H NMR X-ray and mass spectroscopy, in addition to geometrical calculations.

HL ligand was a dark orange colored solid compound, m.p. 190–192 °C and was soluble in common organic solvents. The data of C, H and N content of HL referred to ($C_{16}H_{13}N_3O_3$) are shown in C, 65.09; H, 4.41; N, 14.24, Found: C, 64.89; H, 4.24; N, 13.80 and found to be in good accordance with the calculated value based on the synthetic and proposed structure.

Inspection of IR spectrum of HL revealed that IR spectrum of HL was associated to the aromatic ring system. The absorption band of ligand exhibit a broad band at 3436 cm^{-1} which can be attributed to the υ(OH) group. A medium intensity band at 3180 cm^{-1} is due to the υ(NH) vibrations of the indole ring and two bands at 1714 and 1617 cm^{-1} due to υ(C═O) of isatin moiety and υ(C═N), respectively. The bands observed at 1540, 1251 and 950 cm^{-1} corresponds to the aromatic ring, phenolic (C–O) and (N–N) stretching vibrations, respectively [50].

The ^{1}H NMR spectra of the ligand show two signals at 11.9 and 11.0 ppm corresponding to the N–H and O–H, respectively. The previous two protons disappear in the presence of D_2O. Signal appearing at 8.9 ppm can be attributed to the N═CH. Aromatic proton signals are observed as multiplet in the range 6.9–7.5 ppm. Signal at 3.8 ppm corresponding to the OCH_3.

Molecular docking is a key tool in computer drug design [51]. The focus of molecular docking is to simulate the molecular recognition process. Molecular docking aims to achieve an optimized conformation for both the protein and drug with relative orientation between them such that the free energy of the overall system is minimized. In this context, we used molecular docking between ligand (HL) and crystal structure of *E. coli* (3T88), crystal structure of *S. aureus* (3q8u) and crystal structure of the *C. albicans* (1Q40). The results showed a possible arrangement between ligand (HL) and receptors (3T88, 3q8u and 1Q40). The docking study showed a favorable

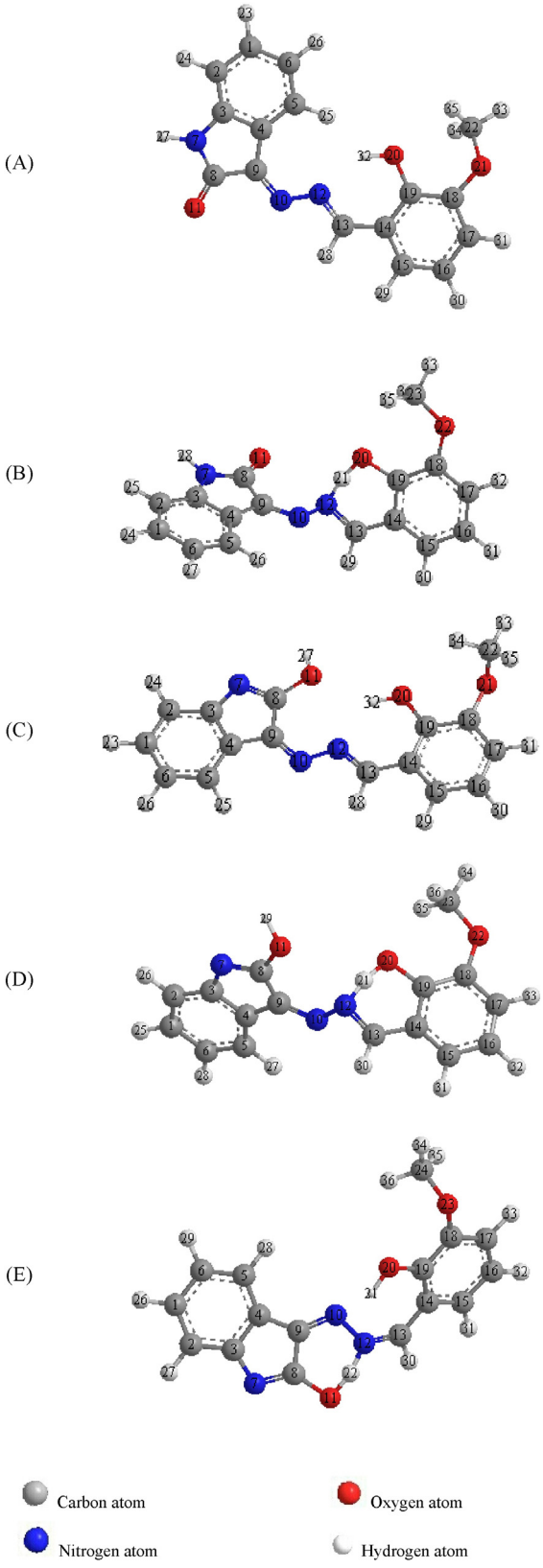

Fig. 5. Molecular structures with atomic numbering for ligand.

interaction between ligand (HL) and the receptors (3T88, 3q8u and 1Q40) as shown in Fig. 2 and the calculated energy is listed in Table 1. According to the results obtained in this study, HB plot curve indicates that the ligand HL binds to the proteins with

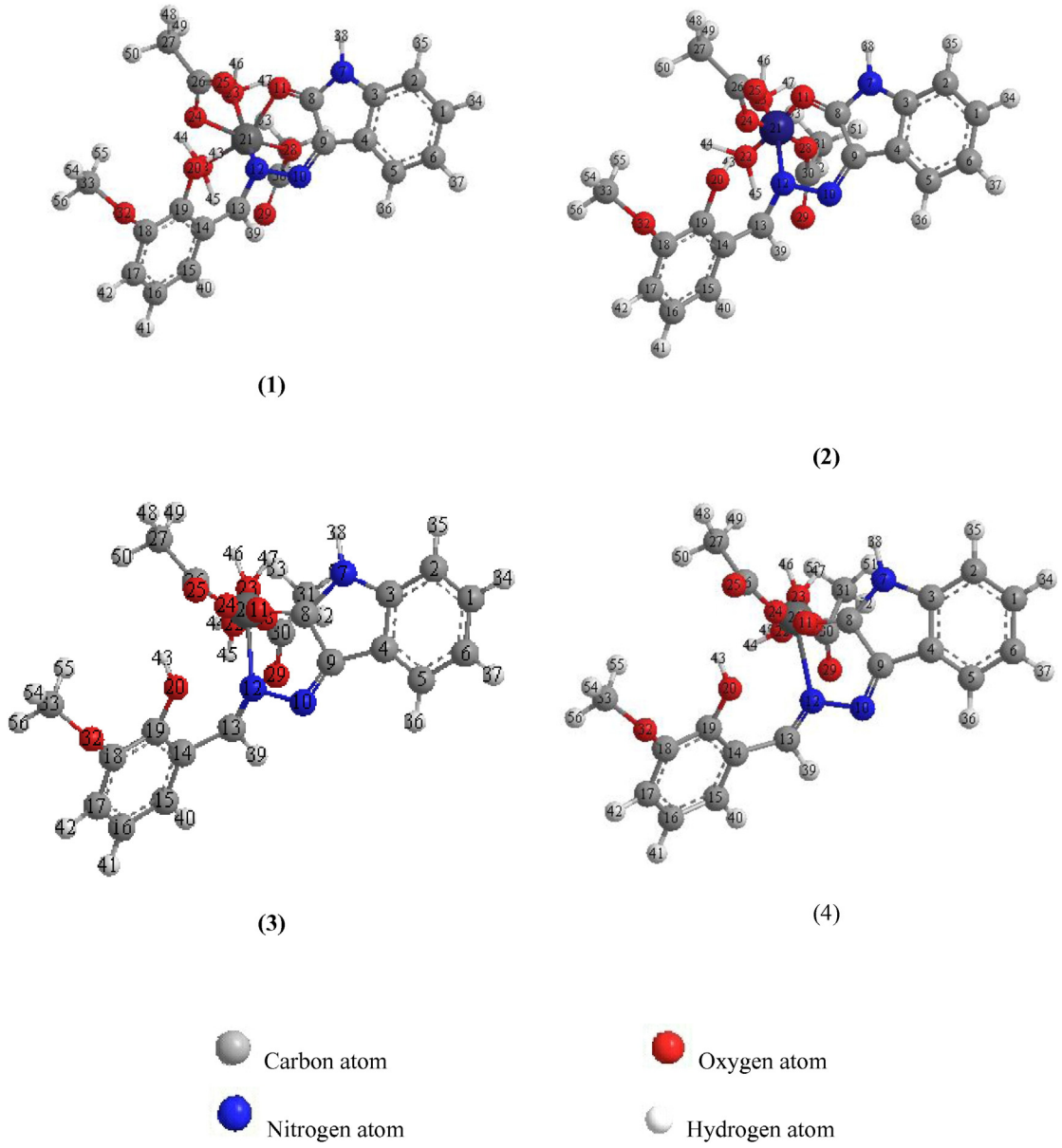

Fig. 6. Molecular structures with atomic numbering for complexes (**1**–**4**).

hydrogen bond interactions and decomposed interaction energies in kcal/mol were exist between ligand (HL) with 3T88, 3q8u and 1Q40 receptors as shown in Fig. 3 (a, b and c). 2D plot curves of docking with ligand (HL) are shown in Fig. 4 (a, b and c). The ligand (HL) shows best interaction with 1Q40 receptor than other receptors.

3.2. Metal complexes

The isolated complexes having general formula $[M(HL)(OAc)_2(OH_2)_2]$ are paramagnetic except Cd(II) is diamagnetic. All Schiff base complexes are highly colored, stable in air, non-hygroscopic in nature and soluble in DMF and DMSO.

The data of elemental analysis for the metal complexes are in good agreement with the calculated values (Table 2) showing that the complexes have 1:1 metal-to-ligand stoichiometry of the $[M(HL)(OAc)_2(OH_2)_2]$. Formation of the complexes can be obtainable in the following reaction.

$$M(CH_3COO)_2 \cdot nH_2O + HL \rightarrow [M(HL)(OAc)_2(OH_2)_2]$$

where M═Cu(II), Co(II), Ni(II) or Cd(II).

For the last reaction the ligand behaves as a neutral and contains two anions (complexes with equivalent anions). The metal(II) complexes were dissolved in DMSO and the molar conductivities of 10^{-3} M of their solution at room temperature were measured. The lower conductance values of the complexes support that non-electrolytic nature of the compounds.

The IR spectra of the metal complexes were similar to each other, except for some slight shift and intensity changes of few vibration peaks caused by different metal(II) ions, indicating that the metal complexes had similar structure.

IR spectra of the complexes clearly indicate the bonding association of the ligand with the metal ion.

In comparison of the spectrum of the free ligand with that of $[Cu(HL)(OAc)_2(OH_2)_2]$, $[Co(HL)(OAc)_2(OH_2)_2]$, $[Ni(HL)(OAc)_2(OH_2)_2]$ and $[Cd(HL)(OAc)_2(OH_2)_2]$ complexes, we found that there are negative shift of both υ(C═O) and υ(C═N), vibrations. While, the υ(OH)

Table 4
Selected geometric bond lengths, bond angles and torsional angles of the HL form (B).

Bond lengths (Å)		Bond angles (°)			
C(23)–H(35)	1.112	N(12)–H(21)–O(20)	166.849	H(28)–N(7)–C(3)	125.092
C(23)–H(34)	1.112	H(35)–C(23)–H(34)	112.743	H(28)–N(7)–C(8)	124.371
C(23)–H(33)	1.113	H(35)–C(23)–H(33)	107.411	C(3)–N(7)–C(8)	110.535
C(17)–H(32)	1.104	H(35)–C(23)–O(22)	110.548	H(27)–C(6)–C(5)	119.442
C(16)–H(31)	1.102	H(34)–C(23)–H(33)	107.903	H(27)–C(6)–C(1)	119.565
C(15)–H(30)	1.102	H(34)–C(23)–O(22)	110.414	C(5)–C(6)–C(1)	120.992
C(13)–H(29)	1.103	H(33)–C(23)–O(22)	107.605	H(26)–C(5)–C(4)	121.218
N(7)–H(28)	1.044	C(18)–O(22)–C(23)	120.513	H(26)–C(5)–C(6)	120.780
C(6)–H(27)	1.103	H(21)–O(20)–C(19)	101.103	C(4)–C(5)–C(6)	118.001
C(5)-H(26)	1.101	O(20)–C(19)–C(14)	115.642	C(3)–C(4)–C(9)	107.242
C(2)–H(25)	1.101	O(20)–C(19)–C(18)	124.485	C(3)–C(4)–C(5)	120.814
C(1)–H(24)	1.103	C(14)–C(19)–C(18)	119.870	C(9)–C(4)–C(5)	131.943
C(3)–C(4)	1.340	O(22)–C(18)–C(19)	126.622	C(4)–C(3)–C(2)	121.590
C(9)–C(4)	1.342	O(22)–C(18)–C(17)	116.717	C(4)–C(3)–N(7)	108.608
C(5)–C(4)	1.339	C(19)–C(18)–C(17)	116.630	C(2)–C(3)–N(7)	129.800
C(6)–C(5)	1.344	H(32)–C(17)–C(18)	118.599	H(25)–C(2)–C(1)	121.305
C(1)–C(6)	1.345	H(32)–C(17)–C(16)	117.914	H(25)–C(2)–C(3)	120.926
C(2)–C(1)	1.344	C(18)–C(17)–C(16)	123.485	C(1)–C(2)–C(3)	117.768
C(3)–C(2)	1.337	H(31)–C(16)–C(17)	120.389	H(24)–C(1)–C(6)	119.675
N(7)–C(3)	1.266	H(31)–C(16)–C(15)	120.147	H(24)–C(1)–C(2)	119.491
C(8)–N(7)	1.266	C(17)–C(16)–C(15)	119.463	C(6)–C(1)–C(2)	120.833
C(9)–C(8)	1.364	H(30)–C(15)–C(16)	120.144	N(7)–C(8)–O(11)	121.827
H(21)–N(12)	1.037	H(30)–C(15)–C(14)	121.470	C(9)–C(8)–O(11)	129.066
O(20)–H(21)	0.998	C(16)–C(15)–C(14)	118.385	H(21)–N(12)–N(10)	113.439
C(18)–O(22)	1.376	C(19)–C(14)–C(15)	122.152	C(13)–N(12)–N(10)	110.496
C(19)–O(20)	1.377	C(19)–C(14)–C(13)	114.494	N(12)–N(10)–C(9)	119.636
C(19)–C(14)	1.355	C(15)–C(14)–C(13)	123.350	C(4)–C(9)–C(8)	104.508
C(18)–C(19)	1.354	H(29)–C(13)–C(14)	122.033	C(4)–C(9)–N(10)	123.146
C(17)–C(18)	1.349	H(29)–C(13)–N(12)	119.087	C(8)–C(9)–N(10)	132.345
C(16)–C(17)	1.340	C(14)–C(13)–N(12)	118.851	N(7)–C(8)–C(9)	109.104
C(15)–C(16)	1.338	H(21)–N(12)–C(13)	103.028		
C(14)–C(15)	1.339	Torsional angles			
C(13)–C(14)	1.351	C(4)–C(9)–N(10)–N(12)	179.076	H(29)–C(13)–C(14)–C(19)	177.168
N(12)–C(13)	1.276	C(2)–C(3)–C(4)–C(9)	179.917	C(17)–C(18)–O(22)–C(23)	167.388
N(10)–N(12)	1.260	H(26)–C(5)–C(4)–C(3)	179.952	C(18)–C(19)–C(14)–C(13)	179.505
C(8)–O(11)	1.212	H(27)–C(6)–C(5)–C(4)	179.997	O(20)–C(19)–C(14)–C(15)	179.335
C(9)–N(10)	1.266	H(24)–C(1)–C(6)–C(5)	179.985	O(22)–C(18)–C(19)–C(14)	179.198
O(22)–C(23)	1.407	H(25)–C(2)–C(1)–C(6)	179.994	H(32)–C(17)–C(18)–C(19)	178.996
		C(8)–N(7)–C(3)–C(2)	179.885	H(30)–C(15)–C(16)–C(17)	179.950
		N(10)–C(9)–C(8)–N(7)	179.891	C(13)–C(14)–C(15)–C(16)	179.781
		C(4)–C(9)–C(8)–O(11)	179.269	N(12)–C(13)–C(14)–C(15)	179.607
		O(20)–H(21)–N(12)–N(10)	116.193		

and υ(NH) vibrations remain at more or less at the same position Table 3, which indicates that they do not participate in coordination to the metal ion. So, the HL acts as a neutral bidentate coordination via υ(C═O) and azomethine nitrogen (C═N) atoms. This observation is further supported by a new bands were observed in 455–495 and 420–440 cm^{-1} regions which assigned to υ(M–O) and υ(M–N), respectively. Coordination of the Schiff base to the metal(II) ion through the azomethine nitrogen atom is expected to reduce the electron density in the azomethine frequency. The band due to azomethine nitrogen υ(C═N) showed a modest decrease in the stretching frequency for the complexes and is shifted to lower frequencies (Table 3) after complexation (bathochromic shift) indicating the coordination of the azomethine [28]. This is further substantiated by shift of a ^{1}H NMR signal for HC═N group. In comparing the position of proton signal in the Cd(II) complex with those of the ligand signal, it can be concluded that all signals are in the expected region and shift only slightly due to the coordination of the ligand to the metal ion. Signal at 4.3 ppm in complex corresponding to water molecules and disappear in the presence of D_2O.

In metal acetate complexes, the acetate group coordinates to the metal ions in a mondentate manner where the difference between the two acetate bands is $\Delta\upsilon > 180\ cm^{-1}$ [52]. Also, the bands of coordinated were observed at ~855 and ~597 cm^{-1}, are assigned to $\rho_r(H_2O)$ and $\rho_w(H_2O)$, respectively. This is supported by results of Ryde [53]. Moreover, strong evidence for the presence or absence of water of crystallization and/or coordinated water supported by the thermogram of all complexes.

3.3. Geometrical structures of the ligand and its metal complexes

Geometrical structure of the ligand (HL) and its metal complexes (**1**–**4**) were calculated by optimizing their bond lengths, bond angels and torsional angles. The geometrical structures of ligand and its metal complexes (**1**–**4**) are presented in Figs. 5 and 6. Selected geometric parameters bond lengths and bond angles and torsional angles of HL and its metal complexes (**1**–**4**) are tabulated in Tables 4–6 (Tables S1–S3 in the supplementary). Both the highest occupied molecular orbital (HOMO) and lowest unoccupied molecular orbital (LUMO) are the main orbital takes part in chemical stability. The HOMO represents the ability to donate an electron, LUMO as an electron acceptor represents the ability to obtain an electron. Molecular orbital structures (HOMO & LUMO) for HL and its metal complexes (**1**–**4**) are presented in Figs. 7 and 8. Primary calculations reveal that the keto form with hydrogen bond (B) is more stable and reactive than other forms (A and C). The existence of hydrogen bond in the optimized structures is observed in the O20–H21–N12 portion. The bond distances, and bond angle values are 0.998, 1.037 Å and 166.849°, respectively. This hydrogen bonding

Table 5
Selected geometric bond lengths and bond angles of the complex (**1**).

Bond lengths (Å)				Bond angles (°)			
C(33)–H(56)	1.11	C(2)–C(3)	1.33	H(56)–C(33)–H(55)	108.02	H(41)–C(16)–C(15)	120.60
C(33)–H(55)	1.11	C(1)–C(2)	1.34	H(56)–C(33)–H(54)	107.97	C(17)–C(16)–C(15)	119.14
C(33)–H(54)	1.11	C(32)–C(33)	1.51	H(56)–C(33)–C(32)	110.64	H(40)–C(15)–C(16)	116.25
C(29)–H(53)	1.11	O(31)–C(32)	1.21	H(55)–C(33)–H(54)	109.24	H(40)–C(15)–C(14)	121.99
C(29)–H(52)	1.11	O(30)–C(32)	1.36	H(55)–C(33)–C(32)	110.43	C(16)–C(15)–C(14)	121.74
C(29)–H(51)	1.11	C(28)–C(29)	1.51	H(54)–C(33)–C(32)	110.44	C(19)–C(14)–C(15)	118.02
C(25)–H(50)	1.11	O(27)–C(28)	1.21	C(33)–C(32)–O(31)	124.34	C(19)–C(14)–C(13)	125.10
C(25)–H(49)	1.11	O(26)–C(28)	1.36	C(33)–C(32)–O(30)	110.77	C(15)–C(14)–C(13)	116.86
C(25)–H(48)	1.11			O(31)–C(32)–O(30)	124.87	H(39)–C(13)–C(14)	112.61
O(23)–H(47)	1.02			Cu(21)–O(30)–C(32)	119.38	H(39)–C(13)–N(12)	115.50
O(23)–H(46)	1.02			H(53)–C(29)–H(52)	107.86	C(14)–C(13)–N(12)	131.65
O(22)–H(45)	1.04			H(53)–C(29)–H(51)	109.13	Cu(21)–N(12)–C(13)	114.49
O(22)–H(44)	1.03			H(53)–C(29)–C(28)	110.69	Cu(21)–N(12)–N(10)	114.90
O(20)–H(43)	0.96			H(52)–C(29)–H(51)	107.84	C(13)–N(12)–N(10)	105.86
C(17)–H(42)	1.10			H(52)–C(29)–C(28)	110.51	Cu(21)–O(11)–C(8)	110.24
C(16)–H(41)	1.10			H(51)–C(29)–C(28)	110.70	N(12)–N(10)–C(9)	116.89
C(15)–H(40)	1.10			C(29)–C(28)–O(27)	124.41	N(10)–C(9)–C(4)	132.69
C(13)–H(39)	1.11			C(29)–C(28)–O(26)	111.19	N(10)–C(9)–C(8)	121.06
N(7)–H(38)	1.04			O(27)–C(28)–O(26)	124.37	C(4)–C(9)–C(8)	105.99
C(6)–H(37)	1.10			Cu(21)–O(26)–C(28)	119.15	O(11)–C(8)–C(9)	125.70
C(5)–H(36)	1.10			H(50)–C(25)–H(49)	110.15	O(11)–C(8)–N(7)	125.02
C(2)–H(35)	1.10			H(50)–C(25)–H(48)	109.13	C(9)–C(8)–N(7)	108.78
C(1)–H(34)	1.10			H(50)–C(25)–O(24)	109.89	H(38)–N(7)–C(8)	124.96
C(14)–C(19)	1.35			H(49)–C(25)–H(48)	109.02	H(38)–N(7)–C(3)	125.21
C(18)–C(19)	1.35			H(49)–C(25)–O(24)	110.40	C(8)–N(7)–C(3)	109.80
C(17)–C(18)	1.34			H(48)–C(25)–O(24)	108.18	H(37)–C(6)–C(1)	119.62
C(16)–C(17)	1.33			C(18)–O(24)–C(25)	113.64	H(37)–C(6)–C(5)	119.41
C(15)–C(16)	1.33			H(47)–O(23)–H(46)	70.02	C(1)–C(6)–C(5)	120.96
C(14)–C(15)	1.34			H(47)–O(23)–Cu(21)	103.10	H(36)–C(5)–C(6)	121.43
O(23)–Cu(21)	1.85			H(46)–O(23)–Cu(21)	96.46	H(36)–C(5)–C(4)	121.10
O(22)–Cu(21)	1.85			H(45)–O(22)–H(44)	161.22	C(6)–C(5)–C(4)	117.45
O(11)–Cu(21)	1.84			H(45)–O(22)–Cu(21)	103.39	C(9)–C(4)–C(5)	132.37
N(12)–Cu(21)	1.36			H(44)–O(22)–Cu(21)	95.27	C(9)–C(4)–C(3)	105.77
Cu(21)–O(30)	1.82			O(23)–Cu(21)–O(22)	77.53	C(5)–C(4)–C(3)	121.84
Cu(21)–O(26)	1.82			O(23)–Cu(21)–O(11)	73.33	N(7)–C(3)–C(4)	109.54
C(18)–O(24)	1.37			O(23)–Cu(21)–N(12)	172.33	N(7)–C(3)–C(2)	129.68
C(19)–O(20)	1.35			O(23)–Cu(21)–O(30)	81.68	C(4)–C(3)–C(2)	120.75
C(13)–C(14)	1.35			O(23)–Cu(21)–O(26)	80.11	H(35)–C(2)–C(3)	120.84
N(12)–C(13)	1.28			O(22)–Cu(21)–O(11)	150.31	H(35)–C(2)–C(1)	121.25
N(10)–N(12)	1.27			O(22)–Cu(21)–N(12)	107.60	C(3)–C(2)–C(1)	117.89
C(8)–O(11)	1.22			O(22)–Cu(21)–O(30)	79.63	H(34)–C(1)–C(6)	119.54
C(9)–N(10)	1.26			O(22)–Cu(21)–O(26)	91.88	H(34)–C(1)–C(2)	119.37
C(9)–C(4)	1.33			O(11)–Cu(21)–N(12)	100.86	C(6)–C(1)–C(2)	121.07
C(8)–C(9)	1.35			O(11)–Cu(21)–O(30)	90.55	C(17)–C(18)–O(24)	119.63
N(7)–C(8)	1.26			O(11)–Cu(21)–O(26)	88.67	H(42)–C(17)–C(18)	119.69
C(3)–N(7)	1.26			N(12)–Cu(21)–O(30)	93.52	H(42)–C(17)–C(16)	119.23
C(6)–C(1)	1.34			N(12)–Cu(21)–O(26)	105.06	C(18)–C(17)–C(16)	121.07
C(5)–C(6)	1.34			O(30)–Cu(21)–O(26)	161.20	H(41)–C(16)–C(17)	120.24
C(4)–C(5)	1.33			H(43)–O(20)–C(19)	111.72	C(19)–C(18)–C(17)	118.91
C(3)–C(4)	1.34			C(14)–C(19)–C(18)	120.88	C(19)–C(18)–O(24)	121.03
O(24)–C(25)	1.41			C(14)–C(19)–O(20)	122.09	C(18)–C(19)–O(20)	117.00

can be named as medium strength hydrogen bonding according to Jeffrey's classification [54] on basis of geometrical parameters. The M–N bond length values for complexes (**1**–**4**) are 1.36, 1.95, 2.13, 2.33 A°, the M–O bond length values for complexes (**1**–**4**) are 1.84, 1.17, 0.60, 0.60 A° and bond angle values for complexes (**1**–**4**) are 100.86, 108.96, 71.01, 62.46°, respectively. Quantum chemical parameters of the ligand and its metal complexes (**1**–**4**) are obtained from calculations such as energies of the highest occupied molecular orbital (E_{HOMO}) and the lowest unoccupied molecular orbital (E_{LUMO}) as listed in Tables 7 and 8. Additional parameters such as HOMO–LUMO energy gap, ΔE^*, absolute electronegativities, χ, chemical potentials, Pi, absolute hardness, η, absolute softness, σ, global electrophilicity, ω, global softness, S, and additional electronic charge, ΔN_{max}, are calculated using the following equations [46,55]:

$$\Delta E = E_{LUMO} - E_{HOMO}. \quad (3)$$

$$\chi = \frac{-(E_{HOMO} - E_{LUMO})}{2}. \quad (4)$$

$$\eta = \frac{E_{LUMO} - E_{HOMO}}{2}. \quad (5)$$

$$\sigma = 1/\eta. \quad (6)$$

$$Pi = -\chi. \quad (7)$$

$$S = \frac{1}{2\eta}. \quad (8)$$

$$\omega = Pi^2/2\eta. \quad (9)$$

$$\Delta N_{max} = -Pi/\eta. \quad (10)$$

Table 6
Selected geometric torsional angles of the complexes (**1**–**4**).

Complex	Torsional angles		Complex	Torsional angles	
(**1**)	C(13)–C(14)–C(19)–C(18)	177.3074	(**2**)	C(13)–C(14)–C(19)–C(18)	179.2946
	C(15)–C(14)–C(19)–O(20)	177.143		C(15)–C(14)–C(19)–O(20)	176.5612
	O(24)–C(18)–C(19)–C(14)	178.3012		O(32)–C(18)–C(19)–C(14)	177.9381
	H(42)–C(17)–C(18)–C(19)	175.7959		H(42)–C(17)–C(18)–C(19)	175.3166
	C(13)–C(14)–C(15)–C(16)	179.6539		H(40)–C(15)–C(16)–C(17)	179.6585
	H(46)–O(23)–Cu(21)–O(30)	136.5789		C(13)–C(14)–C(15)–C(16)	177.9113
	H(47)–O(23)–Cu(21)–O(22)	146.7857		H(46)–O(23)–Co(21)–N(12)	145.6082
	H(44)–O(22)–Cu(21)–N(12)	134.2274		H(46)–O(23)–Co(21)–O(22)	156.1262
	H(45)–O(22)–Cu(21)–O(11)	149.2302		H(47)–O(23)–Co(21)–O(24)	146.9765
	H(45)–O(22)–Cu(21)–O(23)	138.0423		H(44)–O(22)–Co(21)–N(12)	119.7913
	C(8)–O(11)–Cu(21)–O(30)	119.4586		H(45)–O(22)–Co(21)–O(11)	138.8026
	N(10)–N(12)–Cu(21)–O(22)	130.9215		H(45)–O(22)–Co(21)–O(23)	124.6037
	C(13)–N(12)–Cu(21)–O(11)	179.5357		N(10)–N(12)–Co(21)–O(22)	139.4419
	C(13)–N(12)–Cu(21)–O(23)	139.3141		N(10)–N(12)–Co(21)–O(23)	150.1092
	N(12)–Cu(21)–O(26)–C(28)	102.5065		O(28)–Co(21)–O(24)–C(26)	126.8878
	N(12)–C(13)–C(14)–C(15)	176.3601		N(12)–Co(21)–O(24)–C(26)	116.8185
	H(39)–C(13)–C(14)–C(19)	169.3097		N(12)–Co(21)–O(28)–C(30)	108.7413
	N(10)–N(12)–C(13)–C(14)	124.5002		N(12)–C(13)–C(14)–C(15)	179.4755
	N(7)–C(8)–O(11)–Cu(21)	174.2405		H(39)–C(13)–C(14)–C(19)	164.287
	C(4)–C(9)–N(10)–N(12)	160.0564		N(10)–N(12)–C(13)–C(14)	117.6696
	N(10)–C(9)–C(4)–C(3)	176.8675		C(9)–N(10)–N(12)–C(13)	176.5038
	O(11)–C(8)–C(9)–C(4)	169.2884		N(7)–C(8)–O(11)–Co(21)	175.1364
	C(2)–C(3)–N(7)–C(8)	178.8576		C(4)–C(9)–N(10)–N(12)	164.4297
	H(37)–C(6)–C(1)–C(2)	179.9162		N(7)–C(8)–C(9)–N(10)	174.0666
	C(4)–C(5)–C(6)–H(37)	179.8442		O(11)–C(8)–C(9)–C(4)	172.6193
	C(3)–C(4)–C(5)–H(36)	179.9445		C(4)–C(3)–N(7)–H(38)	179.8633
	C(2)–C(3)–C(4)–C(9)	179.1768		C(5)–C(6)–C(1)–H(34)	178.1654
	N(7)–C(3)–C(4)–C(5)	179.0815		H(37)–C(6)–C(1)–C(2)	179.068
	H(35)–C(2)–C(3)–C(4)	179.8064		C(2)–C(3)–C(4)–C(9)	176.0945
	H(34)–C(1)–C(2)–C(3)	179.9188		N(7)–C(3)–C(4)–C(5)	179.7081
	O(30)–C(32)–C(33)–H(56)	175.7019		C(1)–C(2)–C(3)–N(7)	179.0951
	O(31)–C(32)–C(33)–H(54)	116.1123		C(6)–C(1)–C(2)–H(35)	179.804
	Cu(21)–O(30)–C(32)–C(33)	124.5563		C(18)–O(32)–C(33)–H(54)	177.6676
	O(26)–C(28)–C(29)–H(52)	169.7626		O(29)–C(30)–C(31)–H(53)	124.1538
	O(27)–C(28)–C(29)–H(53)	110.5536		O(25)–C(26)–C(27)–H(49)	133.6777
	Cu(21)–O(26)–C(28)–C(29)	123.9927			
	C(18)–O(24)–C(25)–H(48)	179.8117			
(**3**)	C(15)–C(14)–C(19)–O(20)	176.1238	(**4**)	C(15)–C(14)–C(19)–O(20)	172.8237
	O(32)–C(18)–C(19)–C(14)	172.5622		O(32)–C(18)–C(19)–C(14)	167.5563
	H(42)–C(17)–C(18)–C(19)	175.4981		H(42)–C(17)–C(18)–C(19)	175.6287
	H(41)–C(16)–C(17)–C(18)	179.7002		H(41)–C(16)–C(17)–C(18)	178.9144
	H(40)–C(15)–C(16)–C(17)	175.9201		H(40)–C(15)–C(16)–C(17)	173.5522
	C(13)–C(14)–C(15)–C(16)	171.6678		C(13)–C(14)–C(15)–C(16)	168.6457
	H(46)–O(23)–Ni(21)–O(28)	179.0184		H(46)–O(23)–Cd(21)–O(28)	154.7782
	H(47)–O(23)–Ni(21)–O(24)	118.1466		H(47)–O(23)–Cd(21)–O(24)	169.8892
	H(45)–O(22)–Ni(21)–O(23)	124.6884		H(44)–O(22)–Cd(21)–N(12)	108.2902
	C(8)–O(11)–Ni(21)–O(22)	106.4722		C(8)–O(11)–Cd(21)–O(22)	122.2247
	N(10)–N(12)–Ni(21)–O(22)	142.8327		N(10)–N(12)–Cd(21)–O(22)	149.781
	C(13)–N(12)–Ni(21)–O(11)	171.5554		C(13)–N(12)–Cd(21)–O(11)	140.5029
	N(12)–Ni(21)–O(24)–C(26)	112.8263		N(12)–Cd(21)–O(24)–C(26)	137.9811
	N(12)–Ni(21)–O(28)–C(30)	107.9752		O(11)–Cd(21)–O(28)–C(30)	174.9852
	O(11)–Ni(21)–O(28)–C(30)	176.7941		C(19)–C(18)–O(32)–C(33)	100.3046
	H(39)–C(13)–C(14)–C(19)	156.3195		N(12)–C(13)–C(14)–C(15)	175.3075
	N(10)–N(12)–C(13)–C(14)	118.6603		H(39)–C(13)–C(14)–C(19)	148.3114
	Ni(21)–N(12)–C(13)–H(39)	105.4409		N(10)–N(12)–C(13)–C(14)	138.3203
	C(9)–N(10)–N(12)–C(13)	152.4023		Cd(21)–N(12)–C(13)–H(39)	140.9462
	N(7)–C(8)–O(11)–Ni(21)	103.701		C(9)–N(10)–N(12)–C(13)	175.7117
	C(4)–C(9)–N(10)–N(12)	169.3799		C(4)–C(9)–N(10)–N(12)	173.6821
	C(8)–C(9)–C(4)–C(5)	175.357		C(8)–C(9)–C(4)–C(5)	175.0561
	N(7)–C(8)–C(9)–N(10)	172.6868		N(7)–C(8)–C(9)–N(10)	179.8703
	C(3)–N(7)–C(8)–O(11)	148.8826		C(3)–N(7)–C(8)–O(11)	157.8418
	C(4)–C(3)–N(7)–H(38)	176.1996		C(4)–C(3)–N(7)–H(38)	178.3991
	C(5)–C(6)–C(1)–H(34)	176.9551		C(5)–C(6)–C(1)–H(34)	179.4311
	C(4)–C(5)–C(6)–H(37)	175.9867		C(4)–C(5)–C(6)–H(37)	176.6988
	C(3)–C(4)–C(5)–H(36)	176.7826		C(3)–C(4)–C(5)–H(36)	176.8517
	C(2)–C(3)–C(4)–C(9)	173.2048		C(2)–C(3)–C(4)–C(9)	178.5285
	C(1)–C(2)–C(3)–N(7)	174.0119		C(1)–C(2)–C(3)–N(7)	175.8518
	C(6)–C(1)–C(2)–H(35)	176.8316		C(6)–C(1)–C(2)–H(35)	178.2484
	C(18)–O(32)–C(33)–H(54)	176.9101		C(18)–O(32)–C(33)–H(54)	177.4826
	O(28)–C(30)–C(31)–H(52)	170.3058		O(28)–C(30)–C(31)–H(52)	163.286
	O(29)–C(30)–C(31)–H(53)	102.7679		O(29)–C(30)–C(31)–H(53)	102.8081
	O(25)–C(26)–C(27)–H(49)	138.2227		O(25)–C(26)–C(27)–H(49)	142.2531
	Ni(21)–O(24)–C(26)–C(27)	104.8072			

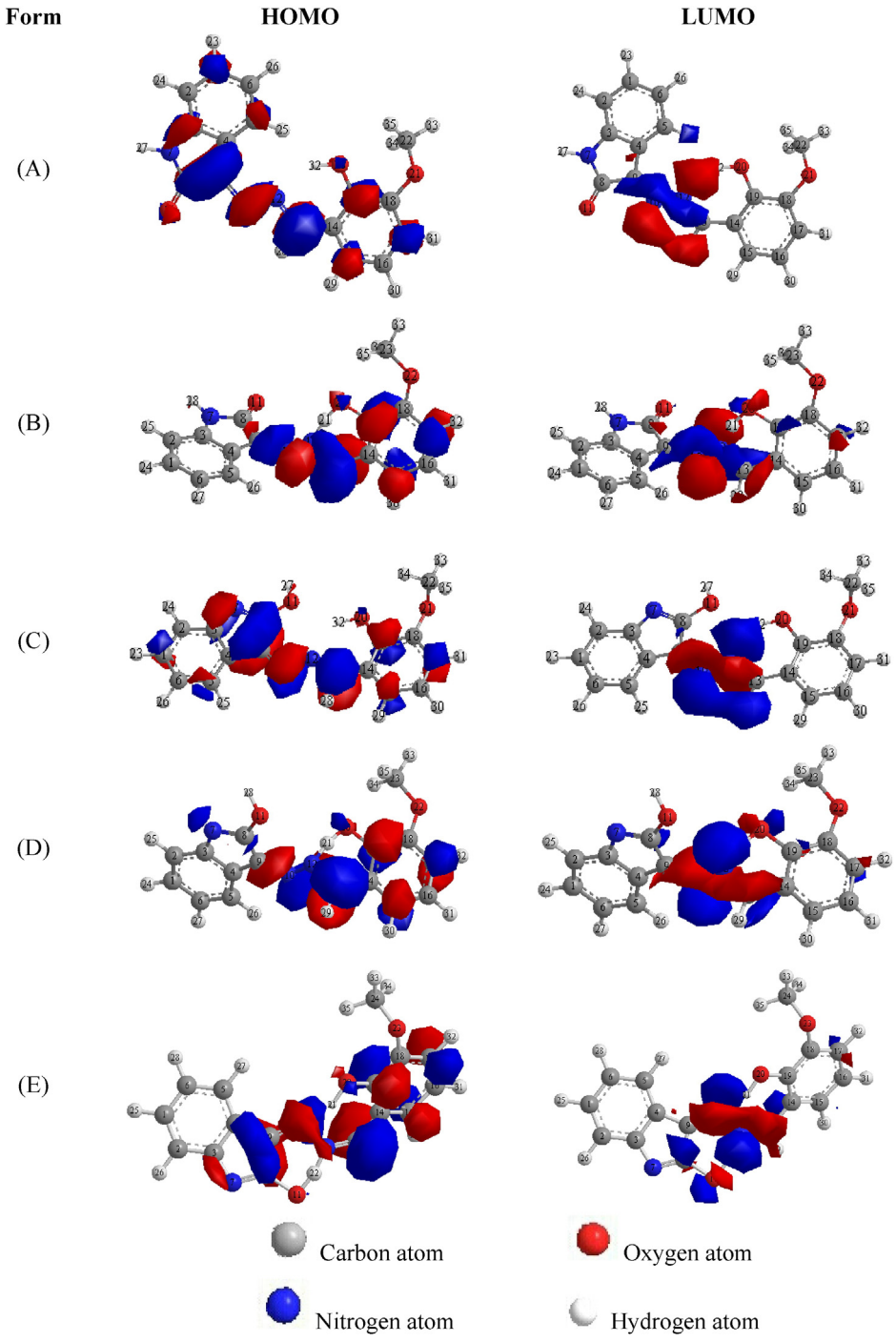

Fig. 7. Molecular orbital structures (HOMO & LUMO) for ligand (HL).

The HOMO and LUMO energy gap, which is an important stability index. The smaller is the value of E_g, the more is the reactivity of the compound [46,55]. It was found that the complex (**1**) i**s** more stable and highly reactive than the other complexes, where the value of ΔE for complexes (**1**–**4**) was found 0.239, 1.540, 2.074 and 4.140 eV, respectively.

3.4. Magnetic moment

The magnetic moment value of the Co(II) complex measured at room temperature is found to be 4.46 B.M. This high spin value of Co(II) complex confirms that the complex has octahedral geometry [56].

The magnetic moment value of the Ni(II) complex is 3.35 B.M. and corresponding to two unpaired electrons. The magnetic moment value is in tune with high spin configuration of octahedral Ni(II) complex [56].

The Cu(II) complex exhibits the magnetic moment value of 1.83 B.M. corresponding to one unpaired electron. This value is higher than the spin-only value, i.e. 1.73 B.M. for one unpaired electron. This reveals that this complex is monomeric in nature without any of metal–metal interaction [56] but with some orbital contribution at room temperature.

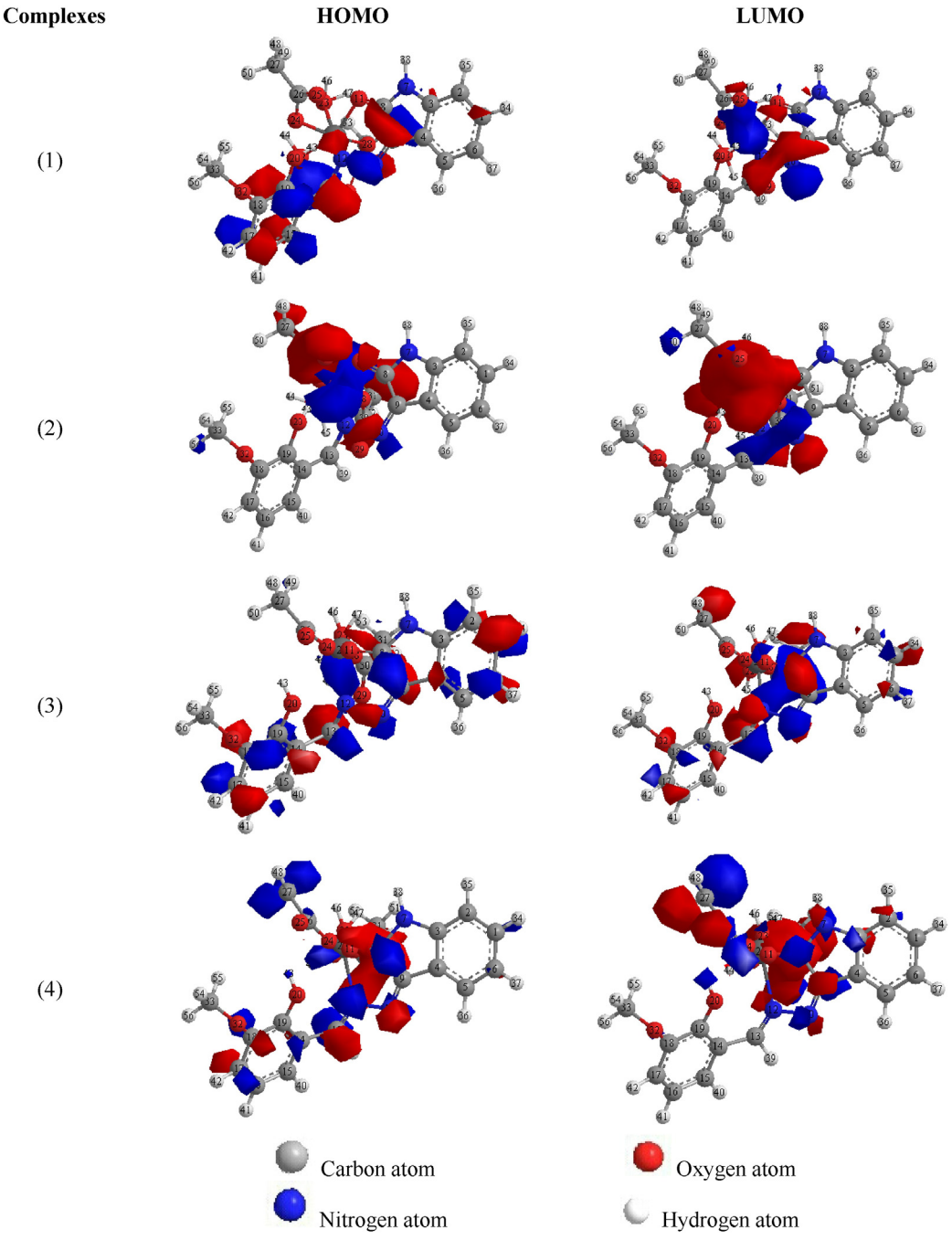

Fig. 8. Molecular orbital structures (HOMO & LUMO) for complexes (**1–4**).

3.5. Electronic spectra

The electronic spectra of the free ligand in DMF showed strong absorption band in the region at 28,900 cm^{-1} and shoulder at 24,630–20,325 cm^{-1} that could be attributed to the $\pi \rightarrow \pi^*$ and $n \rightarrow \pi^*$ transitions in the aromatic ring or azomethine (–C═N) groups for free ligand. In the electronic spectra of the ligand and its metal complexes, the wide range bands were observed due to either

Table 7
The calculated quantum chemical parameters of the ligand (HL).

Form	E_{HOMO} (eV)	E_{LUMO} (eV)	ΔE (eV)	*X* (eV)	η (eV)	σ $(eV)^{-1}$	P_i (eV)	S $(eV)^{-1}$	Ω (eV)	ΔN_{max}
Keto (A)	−5.741	−3.183	2.558	4.462	1.279	0.781	−4.462	0.390	7.783	3.488
Keto hydrogen bond (B)	−6.225	−4.123	2.102	5.174	1.051	0.951	−5.174	0.475	12.735	4.922
Enol (C)	−6.224	−2.659	3.565	4.441	1.782	0.561	−4.441	0.280	5.533	2.491
Enol hydrogen bond (D)	−6.123	−1.973	4.15	4.048	2.075	0.481	−4.048	0.240	3.948	1.950
Enol hydrogen bond (E)	−5.151	−1.310	3.841	3.230	1.920	0.520	−3.230	0.260	2.717	1.682

Table 8
The calculated quantum chemical parameters of the complexes (**1**–**4**).

Complex[a]	E_{HOMO} (eV)	E_{LUMO} (eV)	ΔE (eV)	X (eV)	η (eV)	σ $(eV)^{-1}$	P_i (eV)	S $(eV)^{-1}$	ω (eV)	ΔN_{max}
(**1**)	−4.773	−4.534	0.239	4.6535	0.119	8.368	−4.653	4.184	90.606	38.941
(**2**)	−3.998	−2.458	1.54	3.228	0.77	1.298	−3.228	0.649	6.766	4.192
(**3**)	2.412	4.486	2.074	−3.449	1.037	0.964	3.449	0.482	5.735	−3.325
(**4**)	5.208	9.348	4.14	−7.278	2.07	0.483	7.278	0.241	12.794	−3.515

[a] Numbers given in Table 2.

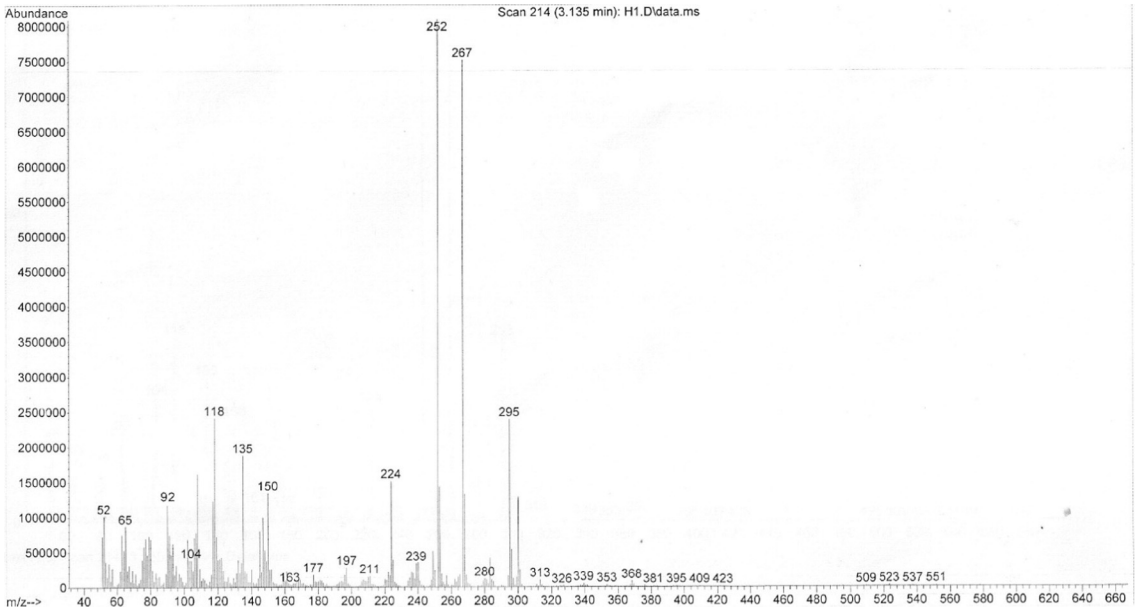

Fig. 9. Mass spectrum of ligand (HL).

the π–π* and n → π* of C═N chromophore or charge-transfer transition arising from π electron interactions between the metal and ligand, which involved either a metal-to-ligand or ligand-to-metal electron transfer [57].

The electronic spectrum of Cu(II) complex exhibits an intense broad band in the range 15,375 cm^{-1} which is attributed to $^2T_{2g} \rightarrow {}^2E_g$ transition, suggesting distorted octahedral geometry [58]. The observed magnetic moment of Cu(II) complex is 1.83 B.M. with the presence of one

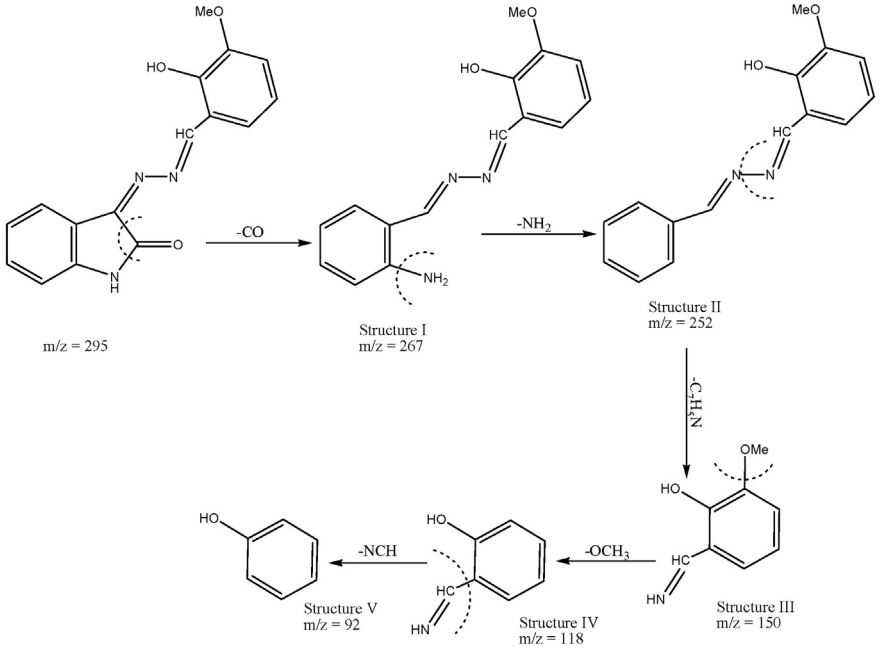

Scheme 2. Fragmentation patterns of ligand (HL).

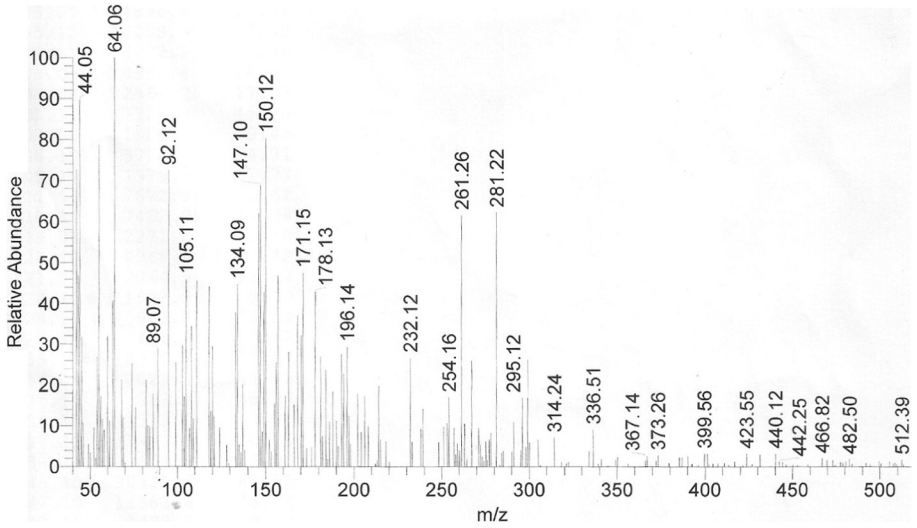

Fig. 10. Mass spectrum of complex (**1**).

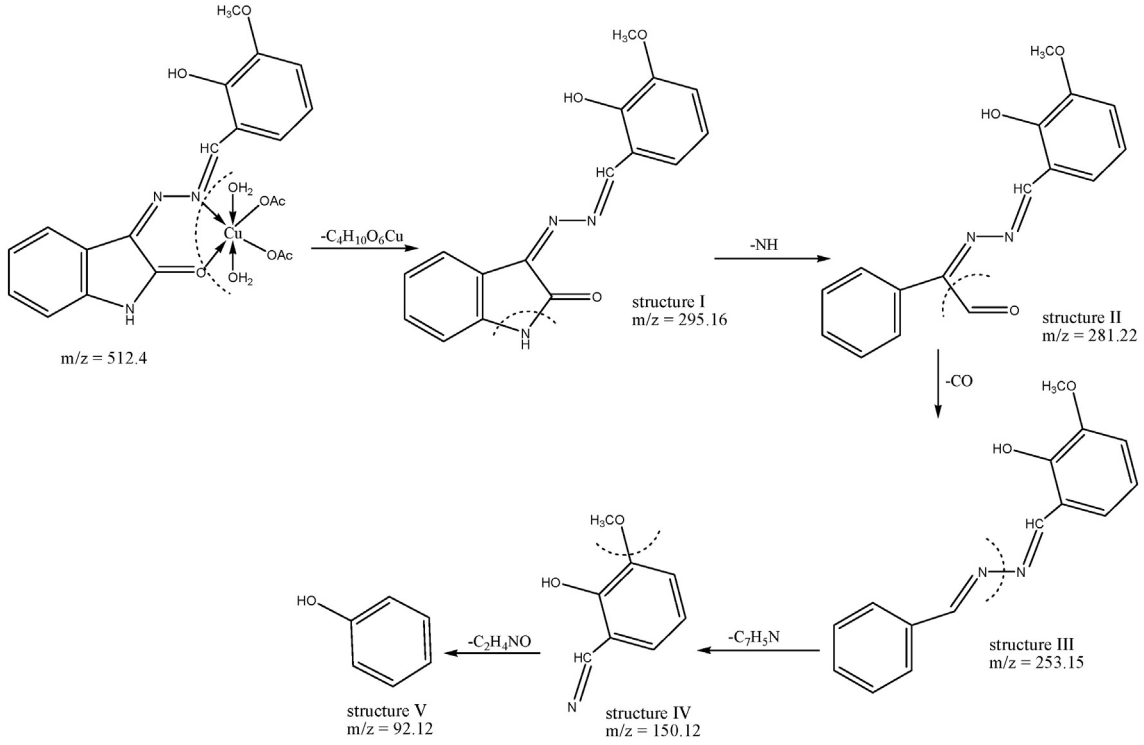

Scheme 3. Fragmentation patterns of complex (**1**).

unpaired electron [56]. The magnetic moment of Co(II) is 4.46 B.M. suggesting a high-spin octahedral configuration [56]. The high value may be due to the orbital contribution.

The Co(II) complex exhibits three bands at 11,760, 18,190 and 26,655 cm^{-1} in the electronic spectrum. The bands can be assigned to $^4T_{1g} \rightarrow {}^4T_{2g}(F)$, $^4T_{1g} \rightarrow {}^4A_{2g}$ and $^4T_{1g}(F) \rightarrow {}^4T_{2g}(P)$ transitions respectively, which are in accordance with its high-spin octahedral geometry [59]. For calculating the Racah parameters, the following equations are used [60].

$$10Dq = 2\upsilon_1 - \upsilon_3 + 15B.$$

$$B = 1/30\left[-(\upsilon_1 - \upsilon_3) \pm \left(-\upsilon_1{}^2 + \upsilon_3{}^2 + \upsilon_1\upsilon_3\right)^{1/2}\right].$$

$$10Dq = 1/2(2\upsilon_2 - \upsilon_3) + 15B.$$

$$B = 1/510\left[7(\upsilon_3 - 2\upsilon_2) \pm 3\left[81\upsilon_3{}^2 - 16\upsilon_2(\upsilon_2 - \upsilon_3)^{1/2}\right]\right].$$

The magnetic moment value of Ni(II) complex is 3.35 B.M. The electronic spectrum exhibits bands at 8.520, 14,520 and 25,000 attributable to $^3A_{2g}(F) \rightarrow {}^3T_{2g}(F)$, $^3A_{2g}(F) \rightarrow {}^3T_{1g}(F)$ and $^3A_{2g}(F) \rightarrow {}^3T_{1g}(P)$ transitions, respectively. These data together with the magnetic moment value are

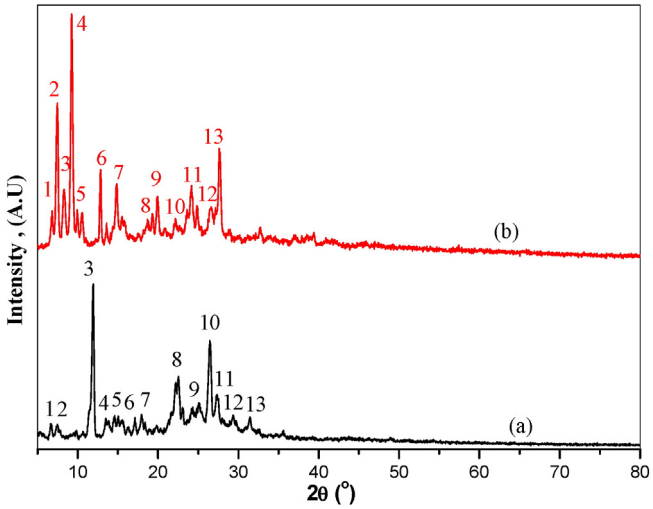

Fig. 11. X-ray diffraction patterns for (a) HL ligand and (b) $[Cu(HL)(OAc)_2(OH_2)_2]$ complex.

suggestive of an octahedral geometry of the complex [59]. The complex of Cd(II) is diamagnetic. In analogy with this described for Cd(II) containing N–O donor Schiff base and according to the empirical formula of this complex. We proposed an octahedral geometry for the Cd(II) complex.

The ESR spectrum of the solid copper(II) complex at room temperature exhibits $g_{II}(2.240) > g_{I}(2.060) > 2.0023$, indicating d_{x2-y2} ground state for tetragonal copper(II) complexes [61]. The value of $g_{av.}(2.12)$, suggests the high covalence property of complex with distorted symmetry [58]. In axial symmetry, the g-value was related to the G-factor by the expression, $G = (g_{II} - 2)/(g_{I} - 2) = 4.12$, which measured the exchange interaction between copper centers in the solid. According to Hathaway and Billing [62]. If the value of G is greater than 4, the exchange interaction between copper(II) centers is negligible, whereas when it is less than 4, a considerable exchange interaction exists in the solid complex. The factor α^2 and β^2 are usually taken as measure of covalency which is evaluated by the expression:

$$\alpha^2 = A_{II}/0.036 + (g_{II}-2.0023) + 3/7(g_{I}-2.0023) + 0.04.$$

$$\beta^2 = (gII-2.0023)E/-8\lambda\alpha^2.$$

where $\lambda = -829\ cm^{-1}$ for the free copper ion and E is the electronic transition energy. The covalency of the in-plane σ-bonding, $\alpha^2 = 1$ indicate the complete ionic character, whereas $\alpha^2 = 0.55$ denotes 100% covalent bonding. The β^2 parameter gave an indication of the covalency of the in-plane π-bonding. The smaller the β^2, the larger is the covalency of the bonding. For the copper(II) complex, the high value of β^2 (1.0) compared to α^2 indicated that the in-plane σ-bonding was more covalent than the in-plane π-bonding.

3.6. Mass spectra

The electron impact mass spectrum of ligand and its metal complexes are recorded and investigated at 70 eV of electron energy. It is obvious that, the molecular ion peaks are in good agreement with their suggested empirical formula as indicated from elemental analysis. The mass spectrum fragmentation mode of ligand (HL) shows the exact mass of 295 corresponding to the formula $C_{16}H_{13}N_3O_3$ (Fig. 9). The ion of m/z = 295 undergoes fragmentation to a stable peak at m/z = 267 by losing CO atoms (structure I) as shown in Scheme 2. The loss of NH_2 leads to the fragmentation with m/z = 252 (structure II). The loss of C_7H_5N atoms leads to the fragmentation with m/z = 150 (structure III). The loss of OCH_3 atoms leads to the fragmentation with m/z = 118 (structure IV). A breakdown of the backbone of ligand gives the fragment (structure V). The mass spectrum fragmentation mode of complex (**1**) shows the exact mass of 512.4 corresponding to the formula $C_{20}H_{23}N_3O_9Cu$ (Fig. 10). The ion of m/z = 512.4 undergoes fragmentation to a stable peak at m/z = 295.16 by losing $C_4H_{10}O_6Cu$ atoms (structure I) as shown in Scheme 3. The loss of NH leads to the fragmentation with m/z = 281.2 (structure II). The loss of CO atoms leads to the fragmentation with m/z = 253.1 (structure III). The loss of C_7H_5N atoms leads to the fragmentation with m/z = 150.1 (structure IV). A breakdown of the backbone of complex gives the fragment (structure V).

Table 9
Crystallographic data for HL and $[Cu(HL)(OAc)_2(OH_2)_2]$.

(HL)				$[Cu(HL)(OAc)_2(OH_2)_2]$			
Sys. triclinic[a]			S.G. p2[b]	Sys. triclinic[a]			S.G. p1[b]
a = 17.079 Å	b = 18.915 Å		c = 11.370 Å	a = 13.585 Å	b = 14.557 Å		c = 9.232 Å
α = 92.84°	β = 96.93°		γ = 94.63°	α = 56.06°	β = 103.28°		γ = 104.82°
Peak no.	2θ (°)	d (Å)	(*hkl*)	Peak no.	2θ (°)	d (Å)	(*hkl*)
1	6.675	13.23	$\bar{1}10$	1	6.809	12.97	$\bar{1}00$
2	7.460	11.84	$1\bar{1}0$	2	7.448	11.85	011
3	11.910	7.42	$0\bar{2}1$	3	9.250	9.55	$1\bar{1}0$
4	13.511	6.54	$2\bar{2}0$	4	9.951	8.88	011
5	14.565	6.07	$1\bar{3}0$	5	10.543	8.38	$\bar{1}11$
6	17.120	5.17	$\bar{3}11$	6	12.846	6.88	$\bar{1}01$
7	17.945	4.93	$0\bar{2}2$	7	14.850	5.96	$0\bar{2}0$
8	22.518	3.94	$\bar{3}31$	8	18.210	4.86	$1\bar{1}1$
9	25.110	3.54	$3\bar{4}1$	9	19.930	4.45	022
10	26.457	3.36	$\bar{4}30$	10	22.178	4.00	032
11	27.354	3.25	123	11	24.150	3.68	$\bar{3}31$
12	29.351	3.04	511	12	27.158	3.28	$\bar{4}10$
13	31.440	2.84	$\bar{4}23$	13	27.657	3.22	$\bar{2}21$

[a] Sys.: System.
[b] S.G.: Space group.

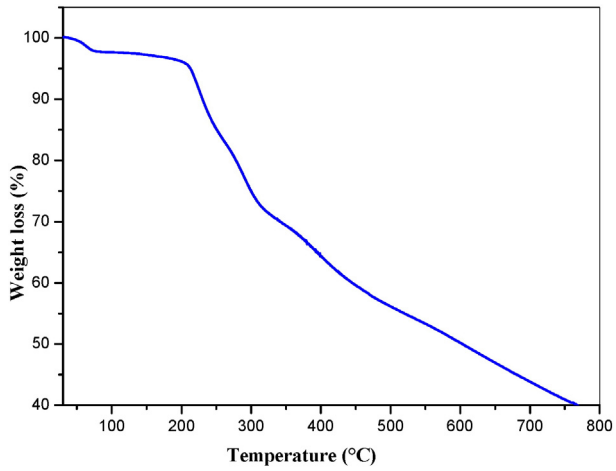

Fig. 12. TGA graph for ligand (HL).

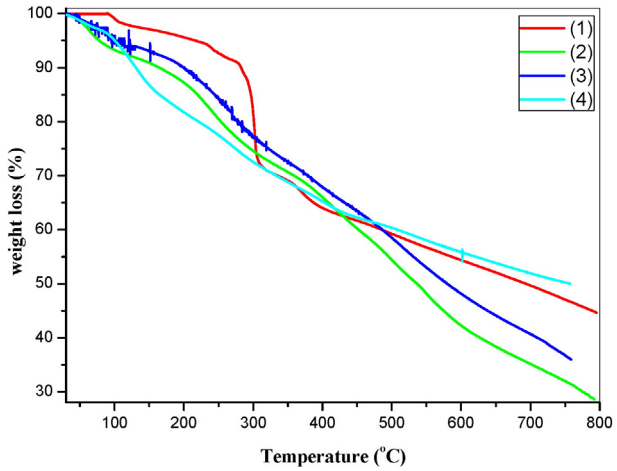

Fig. 13. TGA curves for complexes (**1**–**4**).

3.7. X-ray diffraction analysis

The X-ray diffraction (XRD) patterns of the HL and $[Cu(HL)(OAc)_2(OH_2)_2]$ powder are shown in Fig. 11. The XRD patterns of the HL and $[Cu(HL)(OAc)_2(OH_2)_2]$ show that both of HL and complex are polycrystalline with Triclinic crystal system and structure with space group p2 and p1, respectively. The estimated lattice parameters (a, b, c, α, β and γ), interplanar spacing, d, and Miller indices *hkl*, for the HL and complex are listed in Table 9.

3.8. Thermal analysis

3.8.1. Thermogravimetric analysis of ligand (HL)

The thermal properties of ligand were characterized on the basis of thermogravimetric analysis (TGA) and (DTG) methods in the temperature range 30–800 °C. The TGA curve for ligand is shown in Fig. 12. The temperature intervals and the percentage of loss of masses are listed in Table 10. Ligand shows two decomposition steps, the first stage occur in the temperature range 205–350 °C is attributed to Loss of $C_2H_5N_2O_2$ (Found 30.69%; calc. 30.16%). The second stage in the temperature range 350–759 °C corresponding to loss of C_5H_8NO (Found 31.36%; calc. 33.22%). After 759 °C corresponding to loss of carbon atoms (found 39.59%; calc. 36.61%).

Table 10
Weight losses percentage of ligand and its metal complexes[a].

Compound	Temp. range (°C)	Found mass loss (calc.) %	Assignment
HL	205–350	30.69 (30.16)	Loss of $C_2H_5N_2O_2$
	350–759	31.36 (33.22)	Loss of C_5H_8NO
	>759	39.59 (36.61)	Loss of carbon atoms
(**1**)	128–309	28.02 (30.05)	Loss of $C_4H_{10}O_6$
	309–394	7.67 (8.78)	Loss of HN_2O
	394–795	19.68 (19.90)	Loss of $C_5H_{12}NO$
	>795	44.63 (41.25)	Loss of carbon atoms + CuO
(**2**)	138–323	27.45(30.3)	Loss of $C_4O_6H_{10}$
	323–575	27.85 (27.36)	Loss of $C_6O_2H_7N_2$
	575–763	13.5 (11.02)	Loss of C_3H_6N
	>763	31.20 (31.28)	Loss of carbon atoms + CoO
(**3**)	138–344	27.05 (30.3)	Loss of $C_4H_{10}O_6$
	344–540	18.97 (17.3)	Loss of $C_3H_8N_2O$
	540–758	17.83 (16.35)	Loss of C_4H_5NO
	>758	36.15 (35.97)	Loss of carbon atoms + NiO
(**4**)	120–211	19.35 (16.92)	Loss of $C_2O_4H_7$
	211–446	18.32 (21.55)	Loss of $C_4H_{11}NO_3$
	446–761	12.5 (15.14)	Loss of $C_3H_5N_2O$
	>761	49.83 (46.38)	Loss of carbon atoms + CdO

[a] Numbers given in Table 2.

3.8.2. Thermal analysis of complexes (*1*–*4*)

The TGA of the isolated complexes was taken as a proof for the existing of water molecules as well as the anions in the coordination sphere. The thermal analyses data for the $[M(HL)(OAc)_2(OH_2)_2]$ where (M═Cu(II), Co(II), Ni(II) and Cd(II)) complexes are summarized in Table 10. The TGA curves for complexes are shown in Fig. 13. It can be seen that the TGA curves of the complexes $[M(HL)(OAc)_2(OH_2)_2]$ show loss of masses up to 120 °C above which the dehydration begins. In the first stage, all the complexes (**1**–**4**) loss of the two coordinated water molecules as well as the loss of two acetate groups. The second and third stages are related to decomposition of a parts of the ligand. The final weight losses are due to the decomposition of the rest of the ligand and metal oxides residue.

3.8.3. Calculation of activation thermodynamic parameters

The thermodynamic activation parameters of decomposition processes of the ligand and its metal complexes (**1**–**4**) namely activation energy (Ea), enthalpy (ΔH*), entropy (ΔS*), and Gibbs free energy change of the decomposition (ΔG*) are evaluated graphically by employing the Coast–Redfern [63] and Horowitz–Metzger [64] methods.

3.8.3.1. Coast–Redfern equation. The Coast–Redfern equation, which is a typical integral method, can represent as:

$$\int_0^a \frac{dx}{(1-\alpha)^n} = \frac{A}{\varphi}\int_{T_1}^{T_2} \exp\left(-\frac{E_a}{RT}\right)dt \tag{11}$$

For convenience of integration, the lower limit T_1 usually taken as zero. This equation on integration gives:

$$\ln\left[-\frac{\ln(1-\alpha)}{T^2}\right] = -\frac{E_a}{RT} + \ln\left[\frac{AR}{\varphi E_a}\right] \tag{12}$$

A plot of left-hand side (LHS) against 1/T was drawn (Fig. 14). E_a is the energy of activation in J mol^{-1} and calculated from the slope and A in (s^{-1}) from the intercept value. The entropy of activation (ΔS*) in

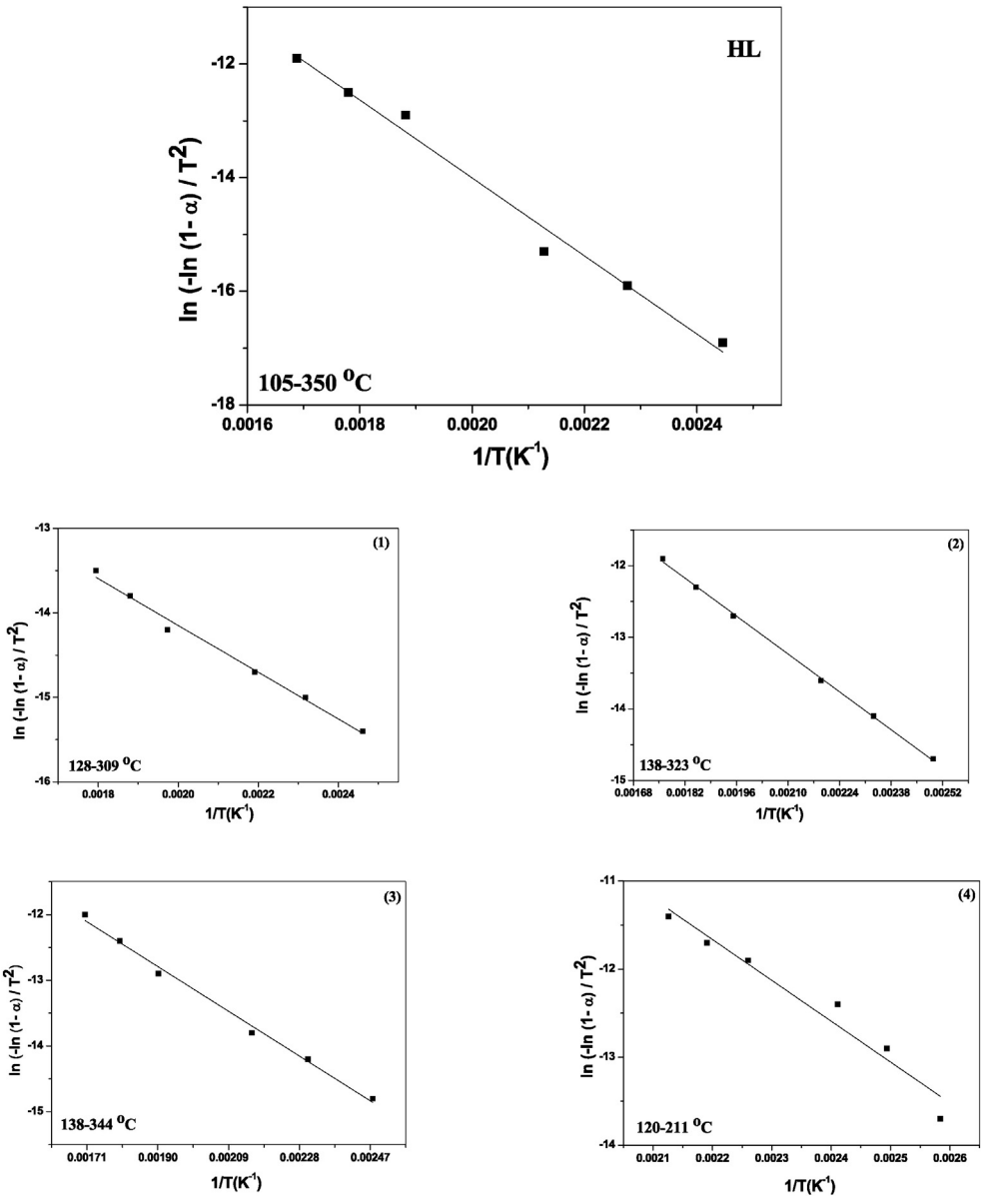

Fig. 14. Coats–Redfern (CR) of the ligand and its metal complexes (**1**–**4**).

$(J \cdot mol^{-1} \cdot K^{-1})$ calculated by using the equation:

$$AS^{*} = 2.303\left[\log\left(\frac{Ah}{k_B T_S}\right)\right]R \tag{13}$$

Where k_B is the Boltzmann constant, h is the Plank's constant and T_s is the TG peak temperature.

3.8.3.2. Horowitz–Metzger equation. The Horowitz–Metzger equation is an illustrative of the approximation methods. These authors derived the relation:

$$\log\left[\frac{1-(1-\alpha)^{1-n}}{1-n}\right] = \frac{E_a\theta}{2.303RT_S^2} \text{ for } n \neq 1 \tag{14}$$

when $n = 1$, the LHS of equation would be $\log[-\log(1-\alpha)]$ (Fig. 15). For a first order kinetic process, the Horowitz-Metzger equation may write in the form:

$$\log\left[\log\left(\frac{W_\alpha}{W_\gamma}\right)\right] = \frac{E_a\theta}{2.303RT_S^2} - \log 2.303 \tag{15}$$

where $\theta = T - T_s$, $w_\gamma = w_\alpha - w$, w_α = mass loss at the completion reaction; w = mass loss up to time t. The plot of log [log (w_α/w_γ)] *vs.* θ was drawn and found to be linear from the slope of which E_a was calculated. The pre-exponential factor, A, calculated from equation:

$$\frac{E_a}{RT_S^2} = \frac{A}{\left[\phi \exp\left(-\frac{E_a}{RT_S}\right)\right]} \tag{16}$$

The entropy of activation, ΔS^*, is calculated from the equation. The enthalpy activation, ΔH^*, and Gibbs free energy, ΔG^*, calculated from:

$$\Delta H^{*} = E_a - RT \tag{17}$$

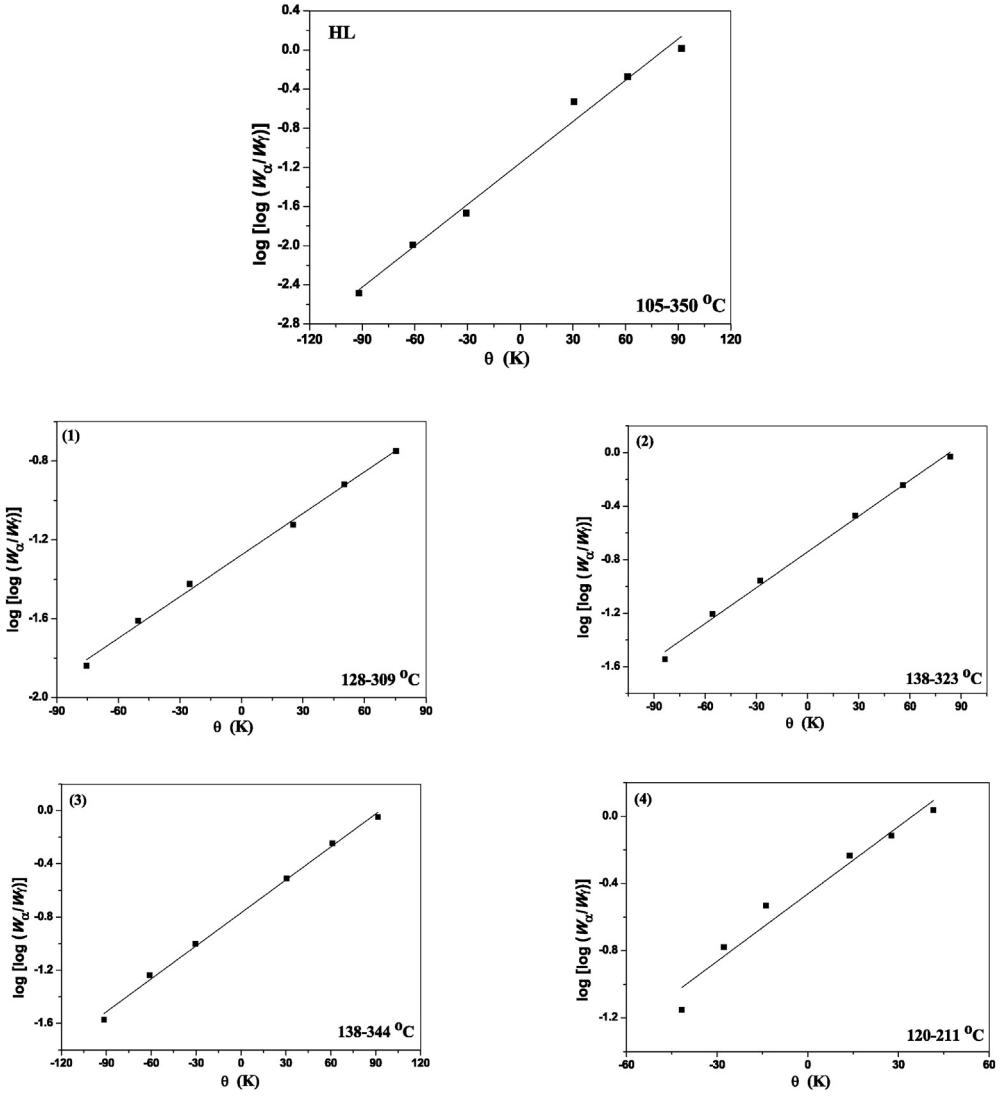

Fig. 15. Horowitz–Metzger (HM) of the ligand and its metal complexes (**1**–**4**).

$$\Delta G^* = \Delta H^* - T\Delta S^* \quad (18)$$

The calculated values of E_a, A, ΔS^*, ΔH^* and ΔG^* for the decomposition steps for ligand and its metal complexes (**1**–**4**) are summarized in Table 11.

3.9. DNA binding studies

Electronic absorption spectroscopy is one of the most universally employed methods to study the binding modes and binding extent of compounds to DNA. DNA usually exhibits hypochromism as a consequence of the intercalation mode, which involves a strong stacking interaction between an aromatic chromophore and the base pairs

Table 11
Kinetic parameters of the ligand and its metal complexes[a].

Compound	Decomposition temperature (°C)	Method	Parameters					Correlation coefficient (r)
			E_a (kJ mol^{-1})	A (s^{-1})	ΔS^* (J mol^{-1} K^{-1})	ΔH^* (kJ mol^{-1})	ΔG^* (kJ mol^{-1})	
(HL)	205–350	CR	57.1	1.31×10^3	-1.90×10^2	52.9	148	0.982
		HM	67.7	9.33×10^4	-1.5410^2	63.5	141	0.985
(**1**)	128–309	CR	23.0	1.25×10^1	-2.66×10^2	19.0	147	0.988
		HM	31.3	9.98	-2.30×10^2	27.3	138	0.995
(**2**)	138–323	CR	31.4	4.76	-2.36×10^2	27.4	142	0.998
		HM	40.1	1.08×10^2	-2.10×10^2	36.1	138	0.994
(**3**)	138–344	CR	29.8	2.26	-2.42×10^2	25.7	146	0.992
		HM	38.8	5.93×10^1	-2.15×10^2	34.7	141	0.996
(**4**)	120–211	CR	38.6	2.70×10^2	-2.01×10^2	35.0	121	0.947
		HM	47.0	4.11×10^3	-1.79×10^2	43.4	120	0.949

[a] Numbers given in Table 2.

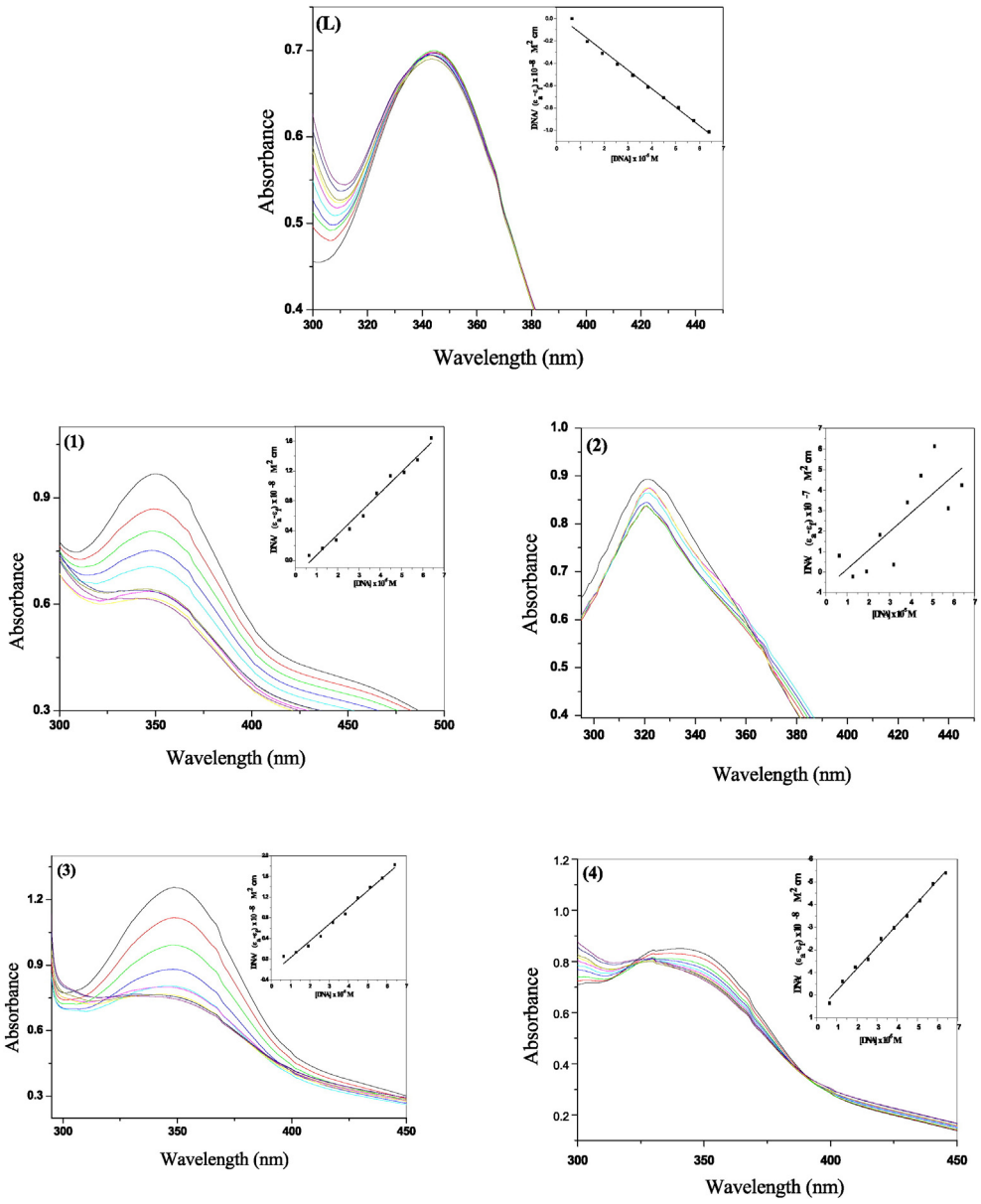

Fig. 16. Absorption spectra of ligand and its metal complexes (**1**–**4**) in buffer pH 7.2 at 25 °C in the presence of increasing amount of CT-DNA. Inset: plot of [DNA]/(ε_a–ε_f) × 10^{-8} M^2 cm versus [DNA] × 10^{-6} M for titration of DNA with ligand and its metal complexes (**1**–**4**).

of DNA. This strong stacking interaction is due to the contraction of calf thymus (CT)-DNA in the helix axis and its conformational changes [65–67]. Absorption titration experiments were performed with fixed concentrations of the ligand (40 μM) and complexes (**1**–**4**) while gradually increasing the concentration of DNA (10 mM) at 25 °C. While measuring the absorption spectra, an equal amount of

Table 12
Effect of ligand and its metal complexes[a] on *S. aureus*, *E. coil* and *C. albicans*.

Compound (mg/ml)	*E. coli*		*S. aureus*		*C. albicans*	
	Diameter of inhibition zone (mm)	% activity index	Diameter of inhibition zone (mm)	% activity index	Diameter of inhibition zone (mm)	% Activity index
(HL)	10	41.7	14	63.6	25	96.1
(**1**)	NA	–	8	36.4	13	50.0
(**2**)	8	33.3	10	45.4	19	73.1
(**3**)	NA	–	7	31.8	18	69.2
(**4**)	5	20.8	16	72.7	21	80.8
Ampicillin	24	100	22	100	NA	–
Colitrimazole	NA	–	NA	–	26	100

Each value was replicated three time.
NA → no activity.
[a] Numbers given in Table 1.

DNA was added to both the compound solution and the reference solution to eliminate the absorbance of DNA itself. We have determined the intrinsic binding constant to CT-DNA by monitoring the absorption intensity of the charge transfer spectral bands 345, 351, 321, 348, 341 nm for the ligand and Cu(III), Co(II), Ni(II) and Cd(II) complexes, respectively. The absorption spectra of these ligand and complexes (**1**–**4**) with increasing concentration of CT-DNA in the range 300–700 nm are shown in Fig. 16.

DNA interaction study by UV–Visible Spectroscopy Electronic absorption spectra were initially used to examine the interaction between ligand and CT-DNA. After interaction with increasing amount of DNA, the absorption spectra of ligand and its metal complexes (**1**–**4**) display clear hypochromism with slight blue shift (~1–2 nm). After the intercalation of the compounds into the base pairs of DNA, the π* orbital of the intercalated compounds are able to couple with the π orbitals of the base pairs, thereby decreasing the π → π* transition energies. These interactions result in the observed hypochromism [68].

The intrinsic binding constant (K_b) of ligand and its metal complexes (**1**–**4**) with DNA was obtained by observing the changes in absorbance of the complexes with increasing concentration of DNA. K_b values for ligand and Cu(II), Co(II), Ni(II) and Cd(II) complexes were found to be 2.99×10^6, 1.34×10^5, 1.19×10^5, 1.10×10^5 and 1.26×10^5 M^{-1}, respectively.

3.10. Structural interpretation

The structures of the complexes of Schiff base HL, with Cu(II), Co(II), Ni(II) and Cd(II) ions are confirmed by elemental analysis, molar conductivity, ^{1}H NMR, UV–vis, IR, mass spectroscopy, X-ray, magnetic measurements and thermal analysis data. Therefore, from the IR spectra, it is concluded that HL behaves as a neutral bidentate ligand with NO sites and coordinated to the metal ions via the azomethine N and carbonyl O. From the molar conductance data of the complexes, it is concluded that the complexes are considered as non-electrolytes. The ^{1}H NMR spectra of the free ligand and its diamagnetic Cd(II) complex shows that the azomethine signal participate in chelation, without proton NH and OH signals of HL and complex displacement and/or coordinated. On the basis of the above observations and from the magnetic and spectral measurements, octahedral geometry is suggested for the investigated complexes are shown in Fig. 1.

3.11. Antimicrobial activity

The antibacterial activity of the Schiff bases may arise from the presence of imine groups and also from the presence of the hydroxyl groups because of their capacity of hydrogen bonding interactions with cellular compartment [69].

The antimicrobial activity of (HL) and metal complexes (**1**–**4**) were tested against bacteria and yeast. More than one test organism was tested to increase the chance of detection of their antimicrobial activities. The used organisms in the present investigations included Gram positive (*S. aureus*), Gram negative (*E. coli*) bacteria and yeast (*C. albicans*). The results of the antimicrobial activities of the synthesized compounds were recorded in Table 12. The zone of inhibition was measured in mm and was compared with a standard drug. DMSO was used as a blank and ampicillin was used as the antibacterial standard and colitrimazole was used as the yeast standard. The results indicate that, these compounds are active in inhibiting the growth of the bacterial and fungal species [70]. All the compounds were tested at 1 mg/mL concentration. The data show that the ligand is the most active than complexes against *E. coli*, with % activity index 41.7. The ligand and Cd(II) complex display good inhibitory properties against the tested *S. aureus* and *C. albicans* with % activity index 63.6 and 72.7 for *S. aureus* and 96.1 and 80.8 for *C. albicans*, respectively.

3.12. Antioxidant assay

In vitro antioxidant activities of all the synthesized compounds were evaluated by 2,2-azinobis-3-ethylbenzothiazoline-6-sulfonic acid (ABTS) cation radical assay as stable free radical which is a conventional and excellent model for assessing the antioxidant activities of hydrogen donating and chain breaking antioxidants [71]. Radical scavenging ability and percentage of inhibition (%) expressed as:

$$\%\ \text{Inhibition} = \frac{A(\text{control}) - A(\text{test})}{A(\text{control})} \times\ 100$$

The results of the antioxidant activities of the synthesized compounds were recorded in Table 13. The ligand exhibited a potent radical scavenging ability with % inhibition value 83.3% which comparable to that of Ascorbic-acid 89%. Compound having –OH (phenolic) group in the phenyl ring as in ligand was found to be the most potent antioxidants [72]. On the other hand, Cd(II) and Co(II) complexes showed moderate antioxidant activity. All complexes of HL represented a lower antioxidant activity compared to its un-complexed compound. In accordance with the cytotoxicity testing results, the complexation decreases the biological activity of the synthesized compound.

3.13. Cytotoxicity assay

The synthesized compounds ligand and its metal complexes (**1**–**4**) were first evaluated with two cancer cell lines (Hepatocellular carcinoma (HepG-2) and mammary gland breast cancer (MCF-7) in vitro by the standard 3-(4,5-dimethylthiazol-2-yl)-2,5-diphenyl tetrazolium

Table 13
Antioxidant assay for the prepared ligand and its metal complexes[a].

Method compounds	ABTS	
	Abs(control) − Abs(test) / Abs(control) × 100	
	Absorbance of samples	% inhibition
Control of ABTS	0.520	0%
Ascorbic-acid	0.057	89.0%
(HL)	0.087	83.3%
(**1**)	0.315	39.4%
(**2**)	0.281	46.0%
(**3**)	0.321	38.3%
(**4**)	0.172	66.9%

[a] Numbers given in Table 2.

Table 14
Evaluation of cytotoxicity of Ligand (HL) and their metal complexes (**1**–**4**) against HepG-2 and MCF-7 cells.

Cell lines	Sample conc.	Compound					
		5-FU	HL	(**1**)	(**2**)	(**3**)	(**4**)
HepG-2	100 μg/ml	8.6	16.3	43.6	38.3	33.9	20.8
	50 μg/ml	17.1	25.1	55.8	50.4	45.8	27.3
	25 μg/ml	24.0	36.7	67.2	62.7	58.1	38.1
	12.5 μg/ml	33.1	48.2	79.3	75.0	68.7	51.7
	6.25 μg/ml	56.8	67.5	93.6	89.6	90.3	72.6
	3.125 μg/ml	70.6	88.9	100	100	100	91.5
	1.56 μg/ml	88.7	100	100	100	100	100
	0 μg/ml	100	100	100	100	100	100
MCF-7	100 μg/ml	5.8	33.3	45.6	41.3	47.3	37.9
	50 μg/ml	10.3	46.2	57.3	52.7	58.5	49.5
	25 μg/ml	16.2	58.4	71.4	64.1	71.7	61.4
	12.5 μg/ml	28.5	69.8	82.5	77.5	82.9	75.8
	6.25 μg/ml	48.4	90.5	97.1	91.3	96.8	91.7
	3.125 μg/ml	62.8	100	100	100	100	100
	1.56 μg/ml	81.6	100	100	100	100	100
	0 μg/ml	100	100	100	100	100	100

bromide (MTT) method. 5-FU used as positive control for comparison. Inhibitory activity against HepG-2 and MCF-7 cell lines was detected by using different concentrations of the tested compounds (i.e., 1.56, 3.125, 6.25, 12.5, 25, 50 and 100 μg/ml) and viability cells (%) were determined by the colorimetric method, data presented in Table 14. The half-inhibitory concentration (IC_{50}) values were calculated from Fig. 17 and summarized in Table 15.

The evaluated compounds were observed to exhibit favorable growth inhibitory activities against tested cell lines in comparison with 5-FU. The ligand and Cd(II) complex exhibited strong cytotoxicities against HepG2 cells IC_{50} values 14.9 ± 1.30 and 17.3 ± 1.28, respectively. Also they exhibited moderate cytotoxicities against MCF-7 cells IC_{50} values 41.4 ± 3.62 and 50 ± 3.72, respectively. Ni(II) complex exhibited moderate cytotoxicity against HepG2 cells IC_{50} values 41.1 ± 3.11. From the above results the ligand and its metal complexes (**1**–**4**) have a better cytotoxic and antitumor activity against (HepG-2) than (MCF-7).

4. Conclusion

The Schiff base derived from isatin, hydrazine hydrate and 2-hydroxy-3-methoxy-benzaldehyde acts as neutral bidentate ligand. Bonding through azomethine nitrogen and oxygen atoms. On the basis of all the spectral data, it is observed that all complexes (**1**–**4**) possess an octahedral geometry. The XRD studies show that both the ligand and copper(II) complex show polycrystalline with Triclinic crystal system. The calf thymus DNA binding activity of the ligand (HL) and its complexes (**1**–**4**) were studied by absorption spectra measurements. The molecular structures of the investigated compounds have been discussed. The thermal properties of the ligand and its complexes (**1**–**4**) were investigated by thermogravimetry analysis (TGA) and different thermodynamic parameters are calculated using Coats–Redfern and Horowitz–Metzger methods. The ligand and its metal complexes (**1**–**4**) were tested against bacterial species, Gram positive (*S. aureus*),

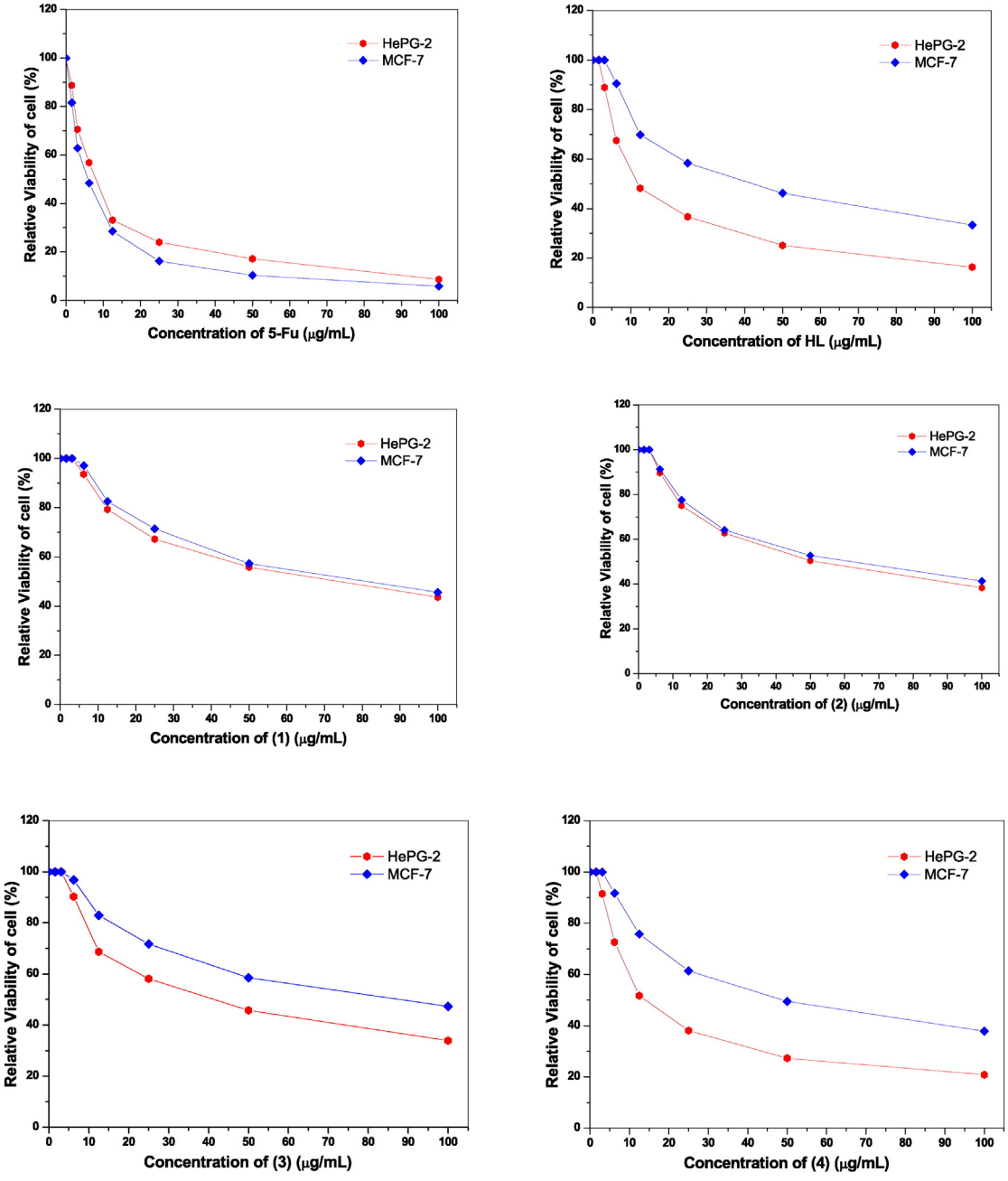

Fig. 17. Cytotoxic and antitumor activity of ligand (HL) and its metal complexes (**1**–**4**) against HePG2 and MCF-7.

Table 15
Evaluation of cytotoxicity of the prepared ligand and its metal complexes[a] against HePG2 and MCF-7 cell.

Compounds	In vitro cytotoxicity IC_{50} (μg/ml)	
	HePG2	MCF-7
5-FU	7.9 ± 0.24	5.6 ± 0.13
(HL)	14.9 ± 1.30	41.4 ± 3.62
(**1**)	66.0 ± 5.15	73.2 ± 4.87
(**2**)	51.4 ± 3.86	57.9 ± 4.17
(**3**)	41.1 ± 3.11	77.9 ± 5.64
(**4**)	17.3 ± 1.28	50.0 ± 3.72

[a] Numbers given in Table 2.

Gram negative (*E. coli*) bacteria and yeast (*C. albicans*). The data show that the ligand is the most active than complexes against *E. coli*. Molecular docking and energy calculations of HL ligand with the receptors of crystal structure of *E. coli* (3T88), crystal structure of *S. aureus* (3q8u) and crystal structure of the *C. albicans* (1Q40) were investigated. It was found that the ligand (HL) shows best interaction with 1Q40 receptor than other receptors.

Appendix A. Supplementary data

Supplementary data to this article can be found online at http://dx.doi.org/10.1016/j.molliq.2016.02.072.

References

[1] R. Lozier, R.A. Bogomolni, W. Stoekenius, J. Biophys. 15 (1975) 955–962.
[2] A.D. Garnovskii, A.L. Nivorozhkin, V.I. Minkin, Coord. Chem. Rev. 126 (1993) 1–69.
[3] C.T. Walsh, W.H. Orme-Johnson, Biochemistry 26 (1987) 4901–4906.
[4] B. Witkop, L.K. Ramachandran, Metabolism 13 (1964) 1016–1025.
[5] R.A. Morton, G.A.J. Pitt, J. Biochem. 59 (1955) 128–134.
[6] M.T. Tarafder, A. Kasbollah, N. Saravan, K.A. Crouse, A.M. Ali, O.K. Tin, J. Biochem. Mol. Biol. Biophys. 6 (2002) 85–91.
[7] R. Pignatello, A. Panico, P. Mazzane, M.R. Pinizzotto, A. Garozzo, P.M. Fumeri, Eur. J. Med. Chem. 29 (1974) 781–785.
[8] J.F.M. Silva, S.J. Garden, A.C. Pinto, Braz. Chem. Soc. 12 (2001) 273–324.
[9] T.O. Olomola, D.A. Bada, C.A. Obafem, Toxicol. Environ. Chem. 91 (2009) 941–946.
[10] B. Bhrigu, D. Pathak, N. Siddiqui, M.S. Alam, W. Ahsan, Int. J. Pharm. Sci. Drug Res. 2 (2010) 229–235.
[11] O. Bekircan, H. Bektas, Molecules 13 (2008) 2126–2135.
[12] A. Jarrahpour, D. Khalili, E. De Clercq, C. Salmi, J.M. Brunel, Molecules 12 (2007) 1720–1730.
[13] I. Chiyanzu, E. Hansell, J. Gut, P.J. Rosenthal, J.H. McKerrow, K. Chibale, Bioorg. Med. Chem. Lett. 13 (2003) 3527–3530.
[14] G. Krishnegowda, A.S.P. Gowda, H.R.S. Tagaram, K.F.S.O. Carroll, R.B. Irby, A.K. Sharma, S. Amin, Bioorg. Med. Chem. 19 (2011) 6006–6014.
[15] P.D.M. Candido-Bacani, M.B.D. Reis, J.M. Serpeloni, T.R. Calvo, W. Vilegas, E.A. Varanda, I.M.D. Syllos-Colus, Mutat. Res. 719 (2011) 47–51.
[16] N. Karalı, O. Guzel, N. Ozsoy, S. Ozbey, A. Salman, Eur. J. Med. Chem. 45 (2010) 1068–1077.
[17] (a) L.S. Feng, M.L. Liu, B. Wang, Y. Chai, X.Q. Hao, S. Meng, H.Y. Guo, Eur. J. Med. Chem. 45 (2010) 3407–3412;
(b) K. Karthikeyan, P.M. Sivakumar, M. Doble, P.T. Perumal, Eur. J. Med. Chem. 45 (2010) 3446–3452.
[18] (a) T.N. Akhaja, J.P.T. Raval, Eur. J. Med. Chem. 46 (2011) 5573–5579;
(b) N. Siddiqui, M.S. Alam, J.P. Stables, Eur. J. Med. Chem. 46 (2011) 2236–2242.
[19] (a) G. Bhaskar, Y. Arun, C. Balachandran, C. Saikumar, P.T. Perumal, Eur. J. Med. Chem. 51 (2012) 79–91.
[20] G. Ermut, N. Karalı, I. Cetin, M. Topcul, S. Birteksoz, Marmara Pharm. J. 17 (2013) 147–154.
[21] J.F.M. Da Silva, S.J. Garden, A.C. Pinto, J. Braz. Chem. Soc. 12 (2001) 273–324.
[22] (a) B. Batanero, F. Barba, Tetrahedron Lett. 47 (2006) 8201–8203;
(b) H. Deng, J.P. Konopelski, Org. Lett. 3 (2001) 3001–3004.
[23] (a) T. Aboul-Fadl, F.A.S. Bin-Jubair, O. Aboul-Wafa, Eur. J. Med. Chem. 45 (2010) 4578–4586;
(b) L. Gupta, N. Sunduru, A. Verma, S. Srivastava, S. Gupta, N. Goyal, P.M.S. Chauhan, Eur. J. Med. Chem. 45 (2010) 2359–2365.
[24] (a) A. Domenech, M.T. Domenech-Carbo, M. Sanchez del Rio, M.L. Vazquez de Agredos Pascual, E. Lima, New J. Chem. 33 (2009) 2371–2379;
(b) E.S.B. Ferreira, A.N. Hulme, H. McNab, A. Quye, Chem. Soc. Rev. 33 (2004) 329–336.
[25] A.M.A. Hassan, Indian J. Chem. 36A (1997) 241–245.
[26] B. Murukan, K. Mohanan, J. Enzyme Inhib, Med. Chem. 22 (2007) 65–70.
[27] S.K. Sridhar, M. Saravanan, A. Ramesh, Eur. J. Med. Chem. 36 (2001) 615–625.
[28] A.Z. El-Sonbati, M.A. Diab, A.A. El-Bindary, M.I. Abou-Dobara, H.A. Seyam, Spectrochim. Acta A 104 (2013) 213–221.
[29] A.A. El-Bindary, A.Z. El-Sonbati, M.A. Diab, Sh.M. Morgan, J. Mol. Liq. 201 (2015) 36–42.
[30] A.Z. El-Sonbati, G.G. Mohamed, A.A. El-Bindary, W.M.I. Hassan, A.K. Elkholy, J. Mol. Liq. 209 (2015) 625–634.
[31] A.A. El-Bindary, A.Z. El-Sonbati, M.A. Diab, E.E. El-Katori, H.A. Seyam, Int. J. Adv. Res. 2 (2014) 493–502.
[32] M.J. Waring, J. Mol. Biol. 13 (1965) 269–282.
[33] M.F. Reichmann, C.A. Rice, C.A. Thomos, P. Doty, J. Am. Chem. Soc. 76 (1954) 3047–3053.
[34] A. Wolfe, G.H. Shimer, T. Meehan, Biochemistry 26 (1987) 6392–6396.
[35] A. Stylianakis, N. Kolocouris, G. Kolocouris, G. Fytas, B. Foscolos, E. Padalko, J. Neyts, D. Clerq, E. Bioorg, Med. Chem. Lett. 13 (2003) 1699–1703.
[36] E. Lissi, B. Modak, R. Torres, J. Escobar, A. Urza, Free Radic. Res. 30 (1999) 471–477.
[37] A.B.A. El-Gazar, A.M.S. Youssef, M.M. Youssef, A.A. Abu-Hashem, F.A. Badria, Eur. J. Med. Chem. 44 (2009) 609–624.
[38] R. Aeschlach, J. Loliger, C.B. Scott, A. Murcia, J. Butler, B. Halliwell, I.O. Aruoma, Food Chem. Toxicol. 32 (1994) 31–36.
[39] T. Mosmann, J. Immunol. Methods 65 (1983) 55–63.
[40] F. Denizot, R. Lang, J. Immunol. Methods 22 (1986) 271–277.
[41] H.J. Mauceri, N.N. Hanna, M.A. Beckett, D.H. Gorski, M.J. Staba, K.A. Stellato, K. Bigelow, R. Heimann, S. Gately, M. Dhanabal, G.A. Soff, V.P. Sukhatme, D.W. Kufe, R.R. Weichselbaum, Nature 394 (1998) 287–291.
[42] A.I. Vogel, Text Book of Quantitative Chemical Analysis, sixth ed. Person Education, India, 2004.
[43] P.W. Selwood, Magnetic Chemistry, Interscience Pub. Inc., New York, 1956.
[44] R. Shirley, "The CRYSFIRE System for Automatic Powder Indexing: User's Manual", the Lattice Press, Guildford, Surrey GU2 7NL, England, 2000.
[45] J. Laugier, B. Bochu, LMGP-Suite Suite of Programs for the Interpretation of X-Ray Experiments, ENSP/Laboratoire Des Materiaux et Du Genie Physique, BP46, 38042, Saint Martin d'Heres, France, 2000.
[46] N.A. El-Ghamaz, M.A. Diab, A.A. El-Bindary, A.Z. El-Sonbati, H.A. Seyam, J. Mater. Sci. Semicond. Process. 27 (2014) 521–531.
[47] N.A. El-Ghamaz, A.Z. El-Sonbati, M.A. Diab, A.A. El-Bindary, G.G. Mohamed, Sh.M. Morgan, Spectrochim. Acta A 147 (2015) 200–211.
[48] T.A. Halgren, J. Comput. Chem. 17 (1998) 490–519.
[49] G.M. Morris, D.S. Goodsell, J. Comput. Chem. 19 (1998) 1639–1662.
[50] K. Nakamoto, Infrared and Raman Spectra of Inorganic and Coordination Compounds, Wiley Interscience, New York, 1986.
[51] A.Z. El-Sonbati, G.G. Mohamed, A.A. El-Bindary, W.M.I. Hassan, M.A. Diab, Sh.M. Morgan, A.K. Elkholy, J. Mol. Liq. 212 (2015) 487–502.
[52] A.Z. El-Sonbati, M.A. Diab, Physico-chemical Studies on the Complexes, LA LAMBERT Acad. Pub. GmbH, Leipzig & Co. KG, 2010, ISBN 978-3-8433-7229-9.
[53] U. Ryde, Biophys. J. 77 (5) (1999) 2777–2787.
[54] G.A. Jeffrey, Introduction to Hydrogen Bonding, Oxford University Press, New York, 1997.
[55] A.Z. El-Sonbati, M.A. Diab, A.A. El-Bindary, Sh.M. Morgan, Spectrochim. Acta A 127 (2014) 310–328.
[56] S. Chandra, L.K. Gupta, Spectrochim. Acta A 61 (2005) 1181–1188.
[57] M. Odabasoglu, F. Arslan, H. Olmez, O. Buyukgungor, Dyes Pigments 75 (2007) 507–515.
[58] A.Z. El-Sonbati, M.A. Diab, A.A. El-Bindary, A.M. Eldesoky, Sh.M. Morgan, Spectrochim. Acta A 135 (2015) 774–791.
[59] A.M.A. Alaghaz, H.A. Bayoumi, Y.A. Ammar, S.A. Aldhlmani, J. Mol. Struct. 1035 (2013) 383–399.
[60] N. Mondal, D.K. Dey, S. Mitra, K.M. Abdul Malik, Polyhedron 19 (2000) 2707–2711.
[61] O.I. Singh, M. Damayant, N.R. Singh, R.K.H. Singh, M. Mohapatra, R.M. Kadam, Polyhedron 24 (2005) 909–916.
[62] B.J. Hathaway, D.E. Billing, Coord. Chem. Rev. 5 (1970) 143–207.
[63] A.W. Coats, J.P. Redfern, Nature 20 (1964) 68–69.
[64] H.W. Horowitza, G. Metzger, Anal. Chem. 35 (1963) 1464–1468.
[65] A.Z. El-Sonbati, A.F. Shoair, A.A. El-Bindary, A.S. Mohamed, J. Mol. Liq. 209 (2015) 635–647.
[66] C.Y. Zhou, J. Zhao, Y.B. Wu, C.X. Yin, P. Yang, J. Inorg. Biochem. 101 (2007) 10–18.
[67] S. Rajalakshmi, T. Weyhermuller, A.J. Freddy, H.R. Vasanthi, B.U. Nair, Eur. J. Med. Chem. 46 (2011) 608–617.
[68] D.S. Raja, N.S.P. Bhuvanesh, K. Natarajan, Inorg. Chim. Acta 385 (2012) 81–93.
[69] L. Shi, H.-M. Ge, S.-H. Tan, H.-Q. Li, Y.-C. Song, H.-L. Zhu, R.-X. Tan, Eur. J. Med. Chem. 42 (2007) 558–564.
[70] S.S. Swathy, R. Selwin Joseyphus, V.P. Nisha, N. Subhadrambika, K. Mohanan, Arab. J. Chem. (2012), http://dx.doi.org/10.1016/j.arabjc.2012.05.004.
[71] L.P. Leong, G. Shui, Food Chem. 76 (2002) 69–75.
[72] K.P. Rakesh, H.M. Manukumar, D. Channe Gowda, Bioorg. Med. Chem. Lett. (2015), http://dx.doi.org/10.1016/j.bmcl.2015.01.010.